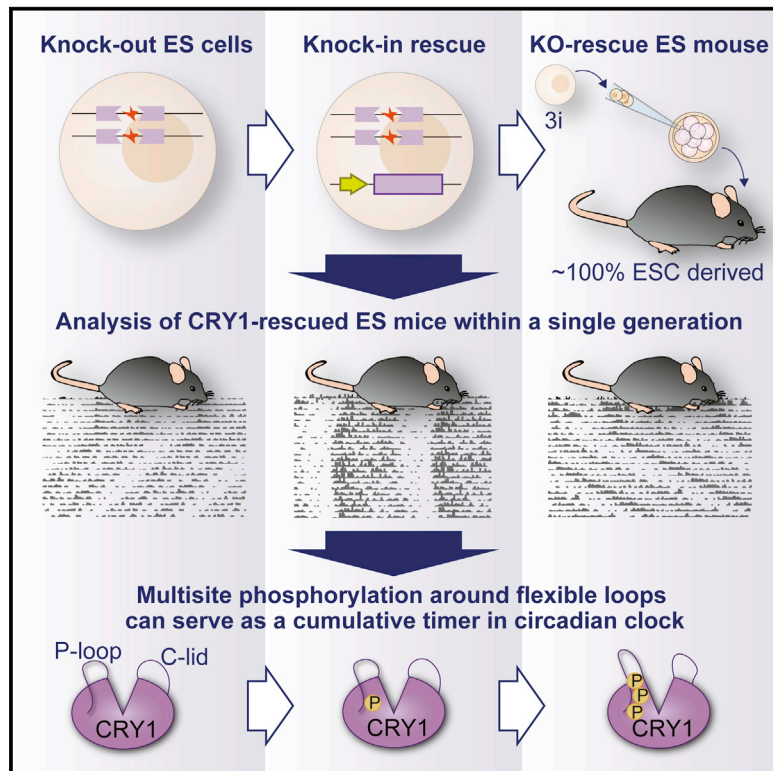


Molecular Cell

Knockout-Rescue Embryonic Stem Cell-Derived Mouse Reveals Circadian-Period Control by Quality and Quantity of CRY1

Graphical Abstract



Authors

Koji L. Ode, Hideki Ukai,
Etsuo A. Susaki, ...,
Masato T. Kanemaki, Hiroshi Kiyonari,
Hiroki R. Ueda

Correspondence

uedah-ky@umin.ac.jp

In Brief

Ode et al. establish an efficient method to conduct gene-rescue experiments in mutant mice. Applying the method to knock in a series of CRY1 mutants into $Cry1^{-/-}:Cry2^{-/-}$ mice, they discover that multisite phosphorylation around the flexible loop domains of CRY1 determine the period length of mammalian circadian clock in vivo.

Highlights

- A KO-rescue ES mouse method was developed to produce 20 different KO-rescue strains
- Multisite phosphorylation of CRY1 can serve as a cumulative timer
- CRY1-PER2 interaction confers a robust circadian rhythmicity in mice
- Flexible loops of CRY1 determine circadian period in mice without a turnover change



Knockout-Rescue Embryonic Stem Cell-Derived Mouse Reveals Circadian-Period Control by Quality and Quantity of CRY1

Koji L. Ode,^{1,2,8} Hideki Ukai,^{2,8} Etsuo A. Susaki,^{1,2,3,8} Ryohei Narumi,^{2,9} Katsuhiko Matsumoto,² Junko Hara,² Naoshi Koide,² Takaya Abe,⁴ Masato T. Kanemaki,^{3,5,6} Hiroshi Kiyonari,^{4,7} and Hiroki R. Ueda^{1,2,10,*}

¹Department of Systems Pharmacology, Graduate School of Medicine, The University of Tokyo, 7-3-1 Hongo, Bunkyo-ku, Tokyo 113-0033, Japan

²Laboratory for Synthetic Biology, RIKEN Quantitative Biology Center, 1-3 Yamadaoka, Suita, Osaka 565-0871, Japan

³PRESTO, Japan Science and Technology Agency (JST), 4-1-8 Honcho, Kawaguchi, Saitama, 332-0012, Japan

⁴Genetic Engineering Team, RIKEN Center for Life Science Technologies, 2-2-3 Minatojima-minamimachi, Chuo-ku, Kobe, Hyogo 650-0047, Japan

⁵Division of Molecular Cell Engineering, National Institute of Genetics, Research Organization of Information and Systems, Yata 1111, Mishima, Shizuoka 411-8540, Japan

⁶Department of Genetics, School of Life Science, SOKENDAI, Mishima, Shizuoka 411-8540, Japan

⁷Animal Resource Development Unit, RIKEN Center for Life Science Technologies, 2-2-3 Minatojima-minamimachi, Chuo-ku, Kobe, Hyogo 650-0047, Japan

⁸Co-first author

⁹Present address: Laboratory of Proteome Research, National Institutes of Biomedical Innovation, Health and Nutrition, Ibaraki, Osaka 567-0085, Japan

¹⁰Lead Contact

*Correspondence: uedah-tky@umin.ac.jp

<http://dx.doi.org/10.1016/j.molcel.2016.11.022>

SUMMARY

To conduct comprehensive characterization of molecular properties in organisms, we established an efficient method to produce knockout (KO)-rescue mice within a single generation. We applied this method to produce 20 strains of almost completely embryonic stem cell (ESC)-derived mice (“ES mice”) rescued with wild-type and mutant *Cry1* gene under a *Cry1*^{-/-}:*Cry2*^{-/-} background. A series of both phosphorylation-mimetic and non-phosphorylation-mimetic CRY1 mutants revealed that multisite phosphorylation of CRY1 can serve as a cumulative timer in the mammalian circadian clock. KO-rescue ES mice also revealed that CRY1-PER2 interaction confers a robust circadian rhythmicity in mice. Surprisingly, in contrast to theoretical predictions from canonical transcription/translation feedback loops, the residues surrounding the flexible P loop and C-lid domains of CRY1 determine circadian period without changing the degradation rate of CRY1. These results suggest that CRY1 determines circadian period through both its degradation-dependent and -independent pathways.

INTRODUCTION

A gene-rescue experiment under mutant background is powerful and has been used in mammalian genetics (Antoch et al., 1997),

but the research procedures often require several generations of animal crosses to obtain genetically modified mice. To overcome these problems, it is ideal if one can perform next-generation mammalian genetics, which can be defined as a production and phenotype analysis of genetically modified mice within a single generation. We previously reported that an injection of three-inhibitor (3i)-treated embryonic stem cells (ESCs) into early stage embryos at eight-cell stage can produce chimera mice with efficient contribution of ESC-derived cells (Kiyonari et al., 2010). Using this technique, it will be plausible to analyze the phenotype of gene-rescued mouse within a single generation by using mutant ESCs as a host cell line for the rescued gene.

Among various applications for this technological platform, the mammalian circadian clock is an ideal model system because of its underlying complex and dynamic molecular networks. The E/E'-box-mediated transcriptional program has a critical role in the core autoregulatory loop of the mammalian circadian clock (Mohawk et al., 2012). In this loop, basic helix-loop-helix (bHLH)-PAS (Per-ARNT-Sim) transcription activators such as BMAL1 and CLOCK form heterodimers that bind to E/E'-box cis-elements in the promoter regions of their target genes including the *Per* and *Cry* genes; CRYs in turn form repressor complexes including PERs and other binding partners (Brown et al., 2005; Duong et al., 2011; Kim et al., 2015) that physically associate with the BMAL1/CLOCK complex to inhibit E/E'-box-mediated transcription. This delayed feedback repression mediated by CRYs, especially CRY1, plays a pivotal role in the cell autonomous circadian oscillation in mammals (Khan et al., 2012; Ukai-Tadenuma et al., 2011).

This model of transcriptional/translational feedback repression leads to theoretical predictions that the increased turnover rate of transcription repressor mRNAs or proteins results in

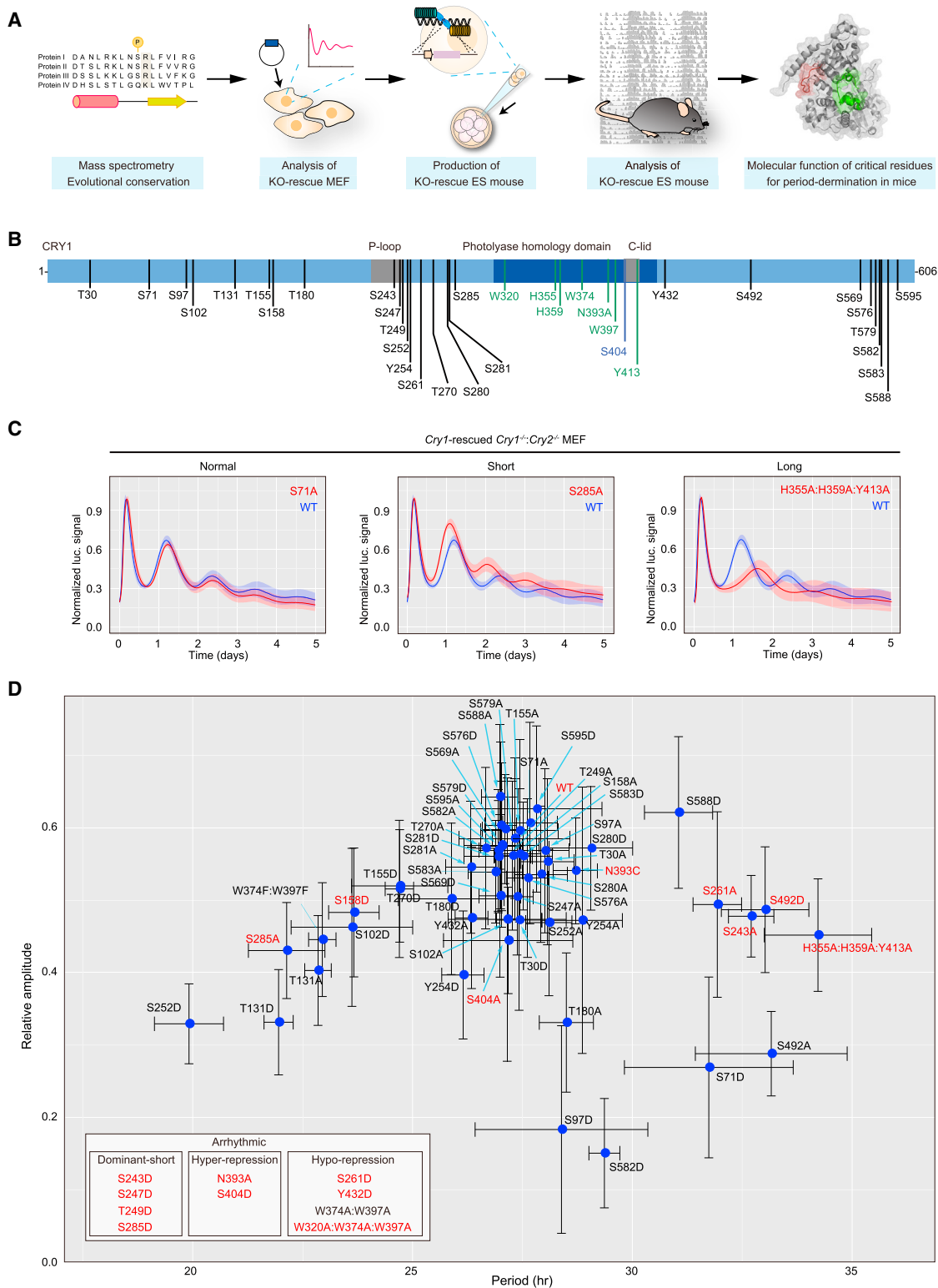


Figure 1. The Phenotype Analysis of KO-Rescue MEFs

(A) A systems framework to reveal the critical residues of CRY1 for controlling the circadian period in vivo.

(B) Identified (black) and predicted (blue) phosphorylation sites, and conserved residues involved in canonical electron-transfer pathway in 6-4 photolyase (green). Identified phosphorylated peptides are shown in Table S1.

(legend continued on next page)

circadian-period shortening (Forger, 2011). Several lines of evidence support this prediction that circadian period of mammalian clocks can be controlled by protein stability of CRY1/2. For example, FBXL3, a component of Skp1-Culin-F-box-protein (SCF) ubiquitin ligase complex that guides CRY1/2 to proteasome-mediated proteolysis, shortens circadian period (Busino et al., 2007; Godinho et al., 2007; Siepka et al., 2007). By contrast, KL001, which binds to the flavin adenine dinucleotide (FAD)-binding pocket of CRY1/2 and stabilizes the protein, lengthens the circadian period (Hirota et al., 2012; Nangle et al., 2013).

However, there are some results that contradict with the theoretical prediction. For example, destabilization of CRY1 by AMPK-dependent phosphorylation should result in the shortening of circadian period, but stimulation of AMPK results in period lengthening (Lamia et al., 2009). A recent chemical-biology study even succeeded to synthesize a compound bound to the CRY1/2 FAD-binding pocket, that shortens the circadian period, but surprisingly, stabilizes CRY1 (Oshima et al., 2015). These results imply that the stability-independent period determination of circadian clocks, demonstrated in other organisms (Larrondo et al., 2015; Nakajima et al., 2005), might be also true for mammalian circadian clocks.

In this study, we established an efficient method to produce knockout (KO)-rescue mice within a single generation (KO-rescue ES mouse method) by the 3i-8-cell method. We then applied this method to the production of 20 strains of different *Cry1* wild-type/mutants knockin mice under a *Cry1*^{-/-}:*Cry2*^{-/-} double mutant background. The mutagenesis of CRY1 revealed that residues surround the flexible P loop and C-lid domains of CRY1 determine the period length of circadian clock, and most of them have only a marginal effect on the degradation rate of CRY1, suggesting the presence of period determination mechanism independent of CRY1's degradation rate. This high-throughput knockin mouse strategy would accelerate circadian and other fields of biology using various mouse strains harboring modified genes or reporters and thus may help to shift the conventional way of mammalian genetics, which depends largely on the crossing of animals.

RESULTS

The Phenotype Analysis of KO-Rescue Mouse Embryonic Fibroblasts

We intended to analyze complex and dynamic molecular networks in organisms by focusing on CRY1 protein in mammalian circadian clocks as a model system (Figure 1A). The first step is the identification of critical residues of CRY1 for circadian-period determination. Phospho-peptides derived from CRY1-overex-

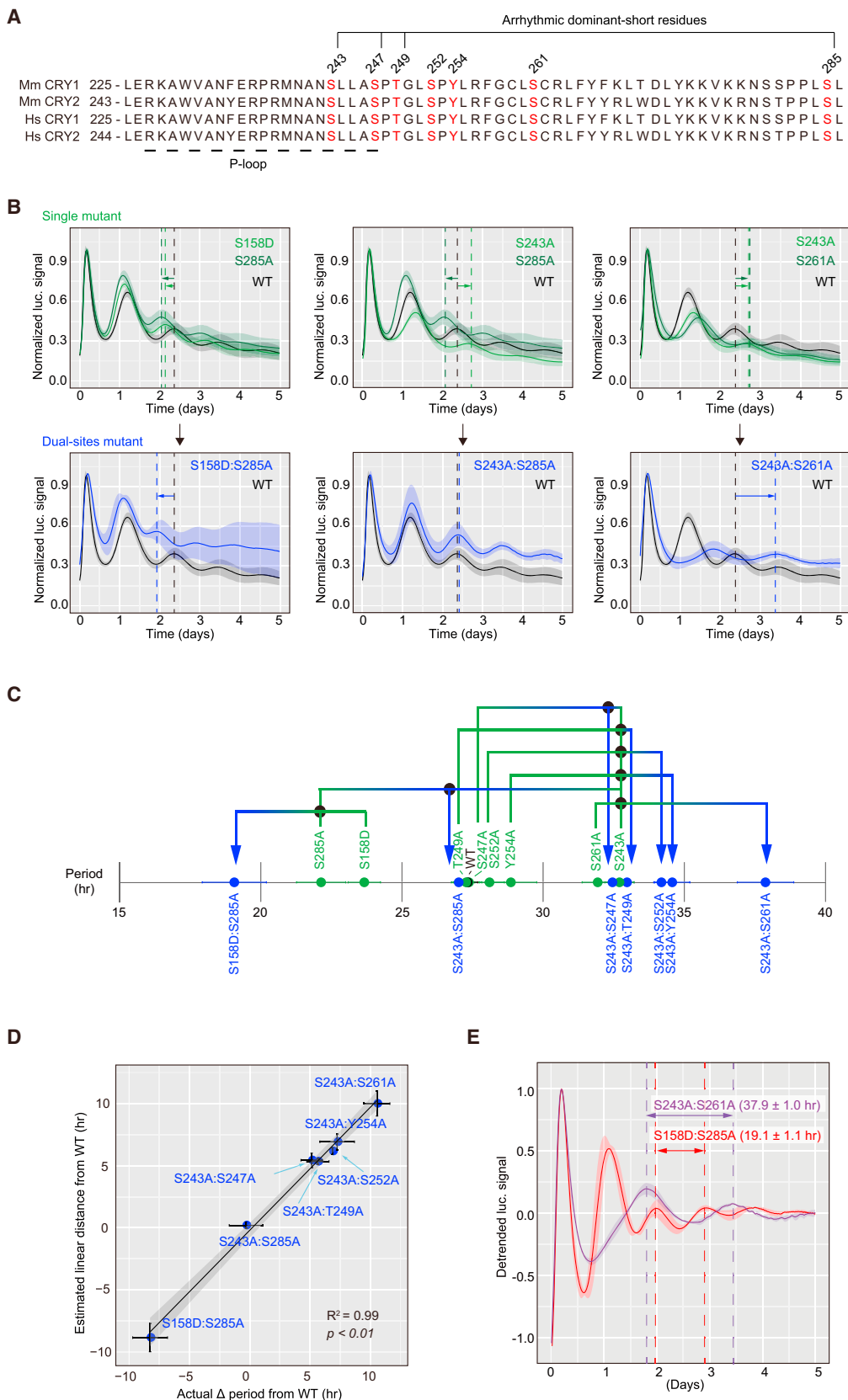
pressed 293T cells were analyzed with mass spectrometer (Figure S1A). We identified 27 phosphorylation sites (Figure 1B; Table S1) including previously reported residues targeted by mitogen-activated protein kinase (MAPK S247) (Sanada et al., 2004), AMPK (S71 and S280) (Lamia et al., 2009), and DNA-PK (S588) (Gao et al., 2013). We did not identify phosphorylation at S404 but included this residue as a possible phosphorylation site based on database prediction as a protein kinase C (PKC)-targeted site (Lamia et al., 2009). Three groups of potential functional residues in CRY1 (tryptophan triplet W320, W374, and W397; histidine/tyrosine triplet H355, H359, and Y413; and asparagine N393) were also selected based on a canonical electron-transfer pathway proposed in its evolutionally most-related protein, 6-4 photolyase (Figure S1B) (Ozturk et al., 2007; Sancar, 2004).

Each phosphorylated residue was then mutated to phosphorylation-mimetic aspartic acid (D) or non-phosphorylation-mimetic alanine (A). The conserved electron-transfer motifs were mutated to alanine. The mutant CRY1 was then expressed in *Cry1*^{-/-}:*Cry2*^{-/-} mouse embryonic fibroblast (MEF) under the control of *Cry1* promoter combined with intronic enhancer Rev-Erb/ROR-binding element (RREs) (Ukai-Tadenuma et al., 2011). The expressed CRY1 rescued circadian rhythmicity in the MEF with various period and amplitude depending on the mutations (Figure 1C). A number of mutants failed to rescue the detectable rhythmicity; we noticed that there are three classes of these arrhythmic mutants, namely, dominant-short, hyperrepression, and hyporepression types (Figure 1D). Each class of mutant affected the circadian rhythmicity in a qualitatively different manner when it was overexpressed in wild-type NIH 3T3 cells (Figure S1C). When wild-type CRY1 was overexpressed in NIH 3T3 cells, the expression greatly suppressed the amplitude of E-box driven reporter without affecting the period length. Arrhythmic hyporepression mutants failed to suppress the amplitude suggesting the reduced transcription-repressor activity. In contrast, mutants classified as arrhythmic hyperrepression further suppressed the amplitude compared with wild-type CRY1, suggesting the enhanced transcription-repression activity. Unlike these classes, arrhythmic dominant-short mutants accelerated the speed of circadian oscillation when they were overexpressed in NIH 3T3 cells. We interpreted that intrinsic period of these arrhythmic dominant-short mutants are extremely short.

The overall in vitro phenotype results are summarized in Figure 1D and Table S2. Although mutation on the conserved electron-transfer motifs caused different effects, we expect that these motifs in mammalian cryptochrome may not have an electron transfer activity, at least in the regulation of circadian rhythmicity, because phenylalanine substitution of tryptophan (W374F:W397F) (23.0 ± 0.3 hr) or cysteine substitution of

(C) Examples of circadian oscillation in *Cry1*^{-/-}:*Cry2*^{-/-} MEF monitored by transiently transfected reporter plasmid expressing destabilized luciferase driven by *Per2* gene's promoter (*P(Per2)-dLuc*). For the *Cry1*^{-/-}:*Cry2*^{-/-} MEF rescue experiments in this and the other figures, the luciferase signal was normalized such that the maximum value of each time course data is one, and shown as average (solid line) ± SD (shade). Note that the same data for wild-type rescue was shown in each panel for comparison.

(D) Period and amplitude of rescued circadian rhythmicity in *Cry1*^{-/-}:*Cry2*^{-/-} MEF was calculated for each mutant CRY1, and shown as average ± SD. The arrhythmic mutants were classified based on the experiments using NIH 3T3 cells as shown in Figure S1C. The value of period and relative amplitude, and number of experiments are shown in Table S2. Wild-type/mutant CRY1 indicated in red were used for KO-rescue ES mouse experiment in Figures 4 and 5. See also Tables S1 and S2 and Figure S1.



(legend on next page)

asparagine N393C (corresponds to insect-specific cryptochromes) (28.7 ± 0.5 hr) support robust circadian oscillations. Many of phosphorylation-mimetic mutation on the phosphorylation cluster near the P loop domain greatly shorten the circadian rhythmicity (e.g., S243D, S247D, T249D, S252D, and S285D). Among all analyzed phosphorylation residues, S243 appears to be the most critical residue for period determination because this site is the only residue that has bidirectional effects on circadian period when mutated to A or D.

Multisite Phosphorylation of CRY1 Can Serve as a Cumulative Timer

We then asked the logic behind the period determination, especially focusing on the phosphorylation cluster near the P loop domain (Figure 2A). If the serial phosphorylation events are triggered by priming phosphorylation at the specific site, then the priming site works as a “switch” and governs the others. In this case, alanine mutation on the priming phosphorylation site is epistatic to the alanine mutation of the other residues. In contrast, if the accumulation of local negative charge additively evokes the response, then the effects of alanine mutations can be cumulative, working as a “timer.” To distinguish these scenarios, we introduced two alanine mutations for a various pair of phosphorylation sites indicated in Figure 2A. We also included one phosphorylation-mimetic mutant (S158D) outside of the region near the P loop domain.

The period of every analyzed CRY1 with mutations in two phosphorylation residues revealed clear additive relationship on the period determination (Figure 2B). The additive rule was applicable not only to the distant pairs of residues (i.e., S158D and S285A) but also to local pairs within the restricted area near the P loop (Figures 2C and 2D; Table S3). This assay also revealed the highly flexible nature of CRY1-dependent period determination at nearly 2-fold dynamic range (Figure 2E). These results suggest that multisite phosphorylation of CRY1 serves as a cumulative timer in mammalian circadian clock.

Because S243 was the only residue that had both shortening and lengthening effects on period, we investigated what kinase is responsible for the phosphorylation at S243. Several algorithms for kinase prediction listed casein kinase I (CKI) as a potential kinase to phosphorylate S243 or downstream S247 (Table S4). Furthermore, we found that one of the responsible kinase for S243 phosphorylation, at least in 293T cells, is CKI δ/ϵ , a major kinase that accelerates the pace of circadian oscillation (Figure S2A; Table S5) (Mohawk et al., 2012).

S243 is conserved in mammalian CRY proteins and plant 6-4 photolyases but is rarely conserved among the other proteins in cryptochrome superfamily (Figure S2B). Phylogeny analysis revealed that serine/threonine and negatively charged aspartic acid and glutamic acid reciprocally emerge among the area surrounding S243 position (Figures S2B–S2D). A phylogenetic theory suggests that phosphorylation activating the protein function tends to be aspartic acid or glutamic acid in the ancestral form (Pearlman et al., 2011). Applying this rationale to mammalian CRY proteins, mammalian cryptochromes for the circadian clock might interchange the static negative charge of D/E with a dynamic phosphorylation site for controlling circadian period.

The Development of a KO-Rescue ES Mouse Method

To directly confirm the in vivo significance of period-determining residues identified in *Cry1*-rescue assay in *Cry1*^{-/-}:*Cry2*^{-/-} MEF, we next conducted *Cry1*-rescue assay under *Cry1*^{-/-}:*Cry2*^{-/-} mice. The coat color of *Cry1*^{-/-}:*Cry2*^{-/-} ES mice was almost identical with the original *Cry1*^{-/-}:*Cry2*^{-/-} mice, suggesting the contamination of host embryo cells, which would result in white coat color, was negligible (Figure 3A). PCR-based genotyping further confirmed that the contamination of cells from the host embryo having a wild-type *Cry2* allele was no more than 0.001% (Figure 3A). Both original *Cry1*^{-/-}:*Cry2*^{-/-} mice and the double-knockout ES mice had arrhythmic behavior (Figure 3B). We then knocked in *Cry1* under the control of *Cry1* promoter including an intronic RRE element (Ukai-Tadenuma et al., 2011) into the ROSA26 locus (Figure 3C; Table S6). During the series of knockin targeting, we used not only a conventional targeting method with on-feeder ESC culture but also a more efficient targeting method with feeder-free ESC culture and TALENs (transcription activator-like effector nucleases) (Figures S3A–S3F) (Sung et al., 2013). These gene-targeting conditions are specified in Table S7.

The *Cry1* cassette introduced in ROSA26 locus rescued circadian rhythmicity in their behavior with slightly different periods depending on the direction of insertion (Figures 3D and 3F; Table S7). We chose the cassette designed to be inserted to ROSA26 locus in antisense direction for subsequent analyses, because their behavioral period in ES mice with a single antisense cassette (24.2–24.3 hr) was closer to the free-running periods of *Cry1*^{+/-}:*Cry2*^{-/-} mice (24.29 hr) (van der Horst et al., 1999). The stringency of the *Cry1* KO-rescue ES mouse method was confirmed by the following two experiments. First, circadian rhythmicity was not observed if *Cry1* gene is driven by

Figure 2. Multisite Phosphorylation of CRY1 Can Serve as a Cumulative Timer

(A) Sequence alignment of P loop and downstream sequence. Indicated residues were used in double mutants in this figure. Mm: *Mus musculus*. Hs: *Homo sapiens*.

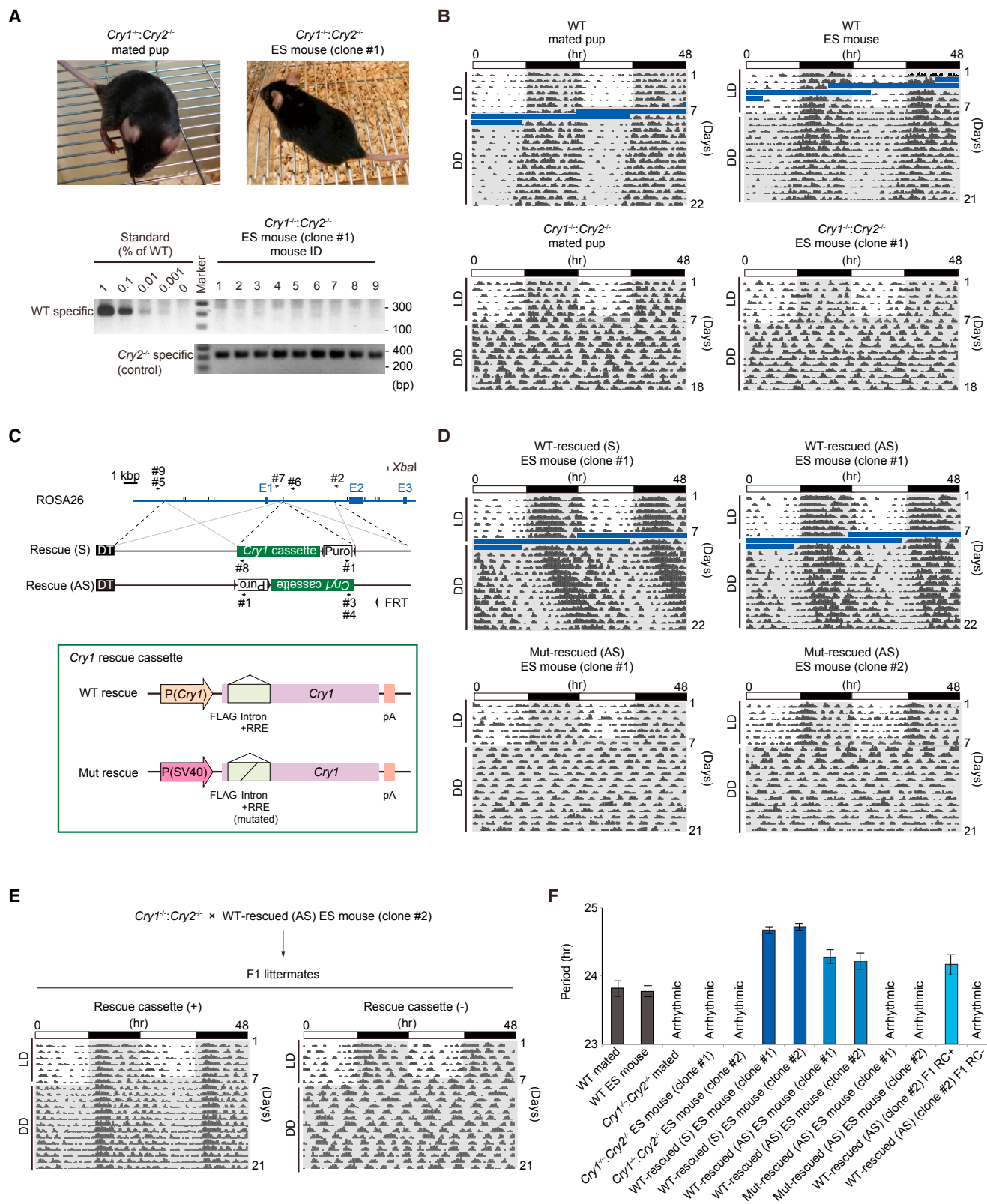
(B) Example of circadian period of wild-type (black), or mutant CRY1 with single (green) or double (blue) phosphorylation residues. The experiment was carried out as in Figure 1. Note that the data of wild-type and of single site mutants (green) were identical data shown in Figures 1C and 1D.

(C) The rescued period lengths for indicated combination of dual-sites mutants were calculated. Note that the periods of single site mutants (green) were identical data shown in Figure 1D.

(D) The effect of double mutants to circadian period is the sum of the effect of individual single mutations. The x axis is the period of rescued *Cry1*^{-/-}:*Cry2*^{-/-} MEF rescued by indicated double mutants as shown in (C). The y axis is the estimated period by adding the period difference between wild-type and individual point mutants. The period lengths are shown as average \pm SD and summarized in Table S3.

(E) Circadian oscillation of CRY1 double mutant showing shortest period (S158D:S285A) and longest period (S243A:S261A). The experiment was carried out as Figure 1, and detrended luciferase signal are shown as average \pm SD.

See also Tables S3, S4, and S5 and Figure S2.



(legend on next page)

non-circadian promoter (Figures 3C and 3D, Mut rescue) (Ukai-Tadenuma et al., 2011). Second, F1 littermates of rescued mice and *Cry1^{-/-}:Cry2^{-/-}* mice showed circadian rhythmicity only if the offspring had *Cry1*-knocked-in allele in the ROSA26 locus (Figure 3E). These results indicate that the behavioral rhythmicity is induced by the *Cry1*-rescue cassette. Note that, for the “Mut rescue” condition, we did not analyze the exact reason of arrhythmicity; it may be due to the altered periodicity for the expression timing of *Cry1* or the altered expression level of *Cry1*. In the following experiments, we used the same (wild-type [WT]) promoter to compare the phenotypes of different *Cry1* mutants.

The Phenotype Analysis of KO-Rescue ES Mice

Seventeen *Cry1* mutants (see Figure 1D, red colored mutants) were selected for the assay of *Cry1*-rescue ES mice. The normal-period mutants in MEFs (N393C and S404A) had almost identical or shorter period in ES mice (24.2 ± 0.1 and 23.9 ± 0.1 hr, respectively) compared with the circadian period of WT-rescued ES mice (24.2 ± 0.1 hr) (Figure 4A). The short-period mutants in MEFs (S158D and S285A) had shorter circadian period in ES mice (23.9 ± 0.1 hr and 23.8 ± 0.1 hr, respectively) (Figure 4B). In contrast, long-period mutants in MEFs (S243A, S492D, and HHY) had significantly longer circadian period in ES mice (24.6 ± 0.05 , 25.4 ± 0.1 , and 26.6 ± 0.3 hr) (Figure 4C).

The arrhythmic dominant-short mutants in MEFs (S243D, S247D, T249D, and S285D) rescued the circadian rhythmicity in KO-rescue ES mice and exhibited markedly shorter period (21.1 ± 0.1 , 22.4 ± 0.1 , 22.7 ± 0.1 , and 22.7 ± 0.1 hr, respectively) (Figure 4D). These results strongly suggest that the intrinsic periods of arrhythmic dominant-short mutants are markedly shorter than that of any other rhythmic mutants in MEFs. In addition, all three arrhythmic hyporepression mutants (S261D, Y432D, and WWW) in MEFs also had arrhythmic phenotype in mice (Figure 4E). These results further strengthen the conclusion that arrhythmic hyporepression mutants are the loss-of-function form of protein and are qualitatively different from arrhythmic dominant-short mutants.

Correlation between the Circadian Phenotype of KO-Rescue MEFs and ES Mice

Overall, KO-rescue ES mice results summarized in Figure 5A demonstrates a striking correlation between circadian periods

observed in MEFs and those observed in KO-rescue ES mice. Note that the magnitude of circadian-period alteration in each CRY1 mutant ES mice from the wild-type was smaller than that of CRY1 mutant MEFs, converging close to 24 hr in KO-rescue ES mice (Figure 5B).

There are several mutants, the phenotypes of which in ES mice are not in line with those of MEFs; S261A mutant had long-period phenotype in MEFs whereas the mutant ES mice had an arrhythmic phenotype (Figure 5C). In addition, the phenotypes of N393A and S404D mutant both of which had arrhythmic hyperrepression phenotypes in MEFs were not reproduced in ES mice: N393A mutant ES mice had a long-period phenotype (25.0 ± 0.4 hr) (Figure 5D), whereas the period of S404D tends to be short in the first 2 weeks after the entry to constant darkness condition and then became longer in the next 2 weeks (Figure 5E). Interestingly, we found that all CRY1 mutants with arrhythmic (S261A, S261D, Y432D, and WWW) or unstable-period (S404D) phenotypes in ES mice had a significant reduction in the interaction with PER2 when these CRY1 mutants were expressed in 293T cells and quantified for the amount of PER2 co-immunoprecipitated with CRY1 (Figure 5F). These results highlight the importance of CRY1-PER2 interaction in stable rhythmicity in vivo.

Correlation of CRY1 Turnover Rate and Circadian Period

To investigate what biochemical properties of CRY1 protein can determine the circadian period and amplitude, we analyzed CRY1's degradation rate (Figure S4A) and transcription-repression activity (Figure S4B). As a result, significant correlation was observed between CRY1 half-life and circadian period and between CRY1 repression activity and circadian amplitude but not for other combinations (Figure S4C). These results are consistent with the canonical relationship between CRY1 degradation and circadian period (Forger, 2011) and between CRY1 repression activity and circadian amplitude (Khan et al., 2012).

To our surprise, a number of mutants had altered circadian period without significant changes in protein half-life (Figure 6A, red circles). Of note, a group of long period mutants (HHY, S492D, S492A, and S243A) had no significant change in protein stability, but their period was significantly longer than the most stable mutant S588D (Gao et al., 2013). Also, it is notable that the arrhythmic dominant-short mutants (S243D, S247D,

Figure 3. The Development of a KO-Rescue ES Mouse Method

(A) 3i-cultured *Cry1^{-/-}:Cry2^{-/-}* ESCs were derived from B6-backcrossed *Cry1^{-/-}:Cry2^{-/-}* strain (van der Horst et al., 1999). ESC clones producing male ES mouse with black coat color were selected. Contamination of host embryo cells was evaluated by semiquantitative genomic PCR for *Cry2* locus with primers specific to wild-type or *Cry2^{-/-}* allele.

(B) Representative actograms of mated pups (wild-type or *Cry1^{-/-}:Cry2^{-/-}* C57BL/6) and ES mice derived from ESCs of wild-type or *Cry1^{-/-}:Cry2^{-/-}* C57BL/6. Shaded regions indicate dark phase. Time windows marked as blue line indicate system shutdown due to the electric outage of the mouse facility.

(C) A structure of *Cry1*-rescue cassette and targeted ROSA26 locus. “WT rescue” cassette drives *Cry1* expression by promoter of *Cry1* gene and intronic RRE element (Ukai-Tadenuma et al., 2011). In the “Mut rescue” cassette, the promoter is swapped to SV40 promoter and the sequences of intronic RRE are mutated. Arrows with numbers indicate PCR primers for ESC screenings and genome integrity confirmations, summarized in Table S6. AS, antisense, pA, poly-A tail; S, sense.

(D) Representative actograms of *Cry1^{-/-}:Cry2^{-/-}* ES mice rescued with WT rescue cassette in sense (S) or antisense (AS) direction, and Mut rescue cassette in antisense (AS) direction.

(E) Representative actograms of F1 offspring obtained by crossing the rescued ES mice with *Cry1^{-/-}:Cry2^{-/-}* strain. The offspring harboring the *Cry1*-rescue cassette (indicated as “+”) at the ROSA26 locus showed circadian behavioral rhythmicity.

(F) Summary of the quantified period of circadian behavioral rhythmicity shown as average \pm SD (during DD condition). The period lengths and gene-targeting conditions are summarized in Table S7.

See also Tables S6 and S7 and Figure S3.

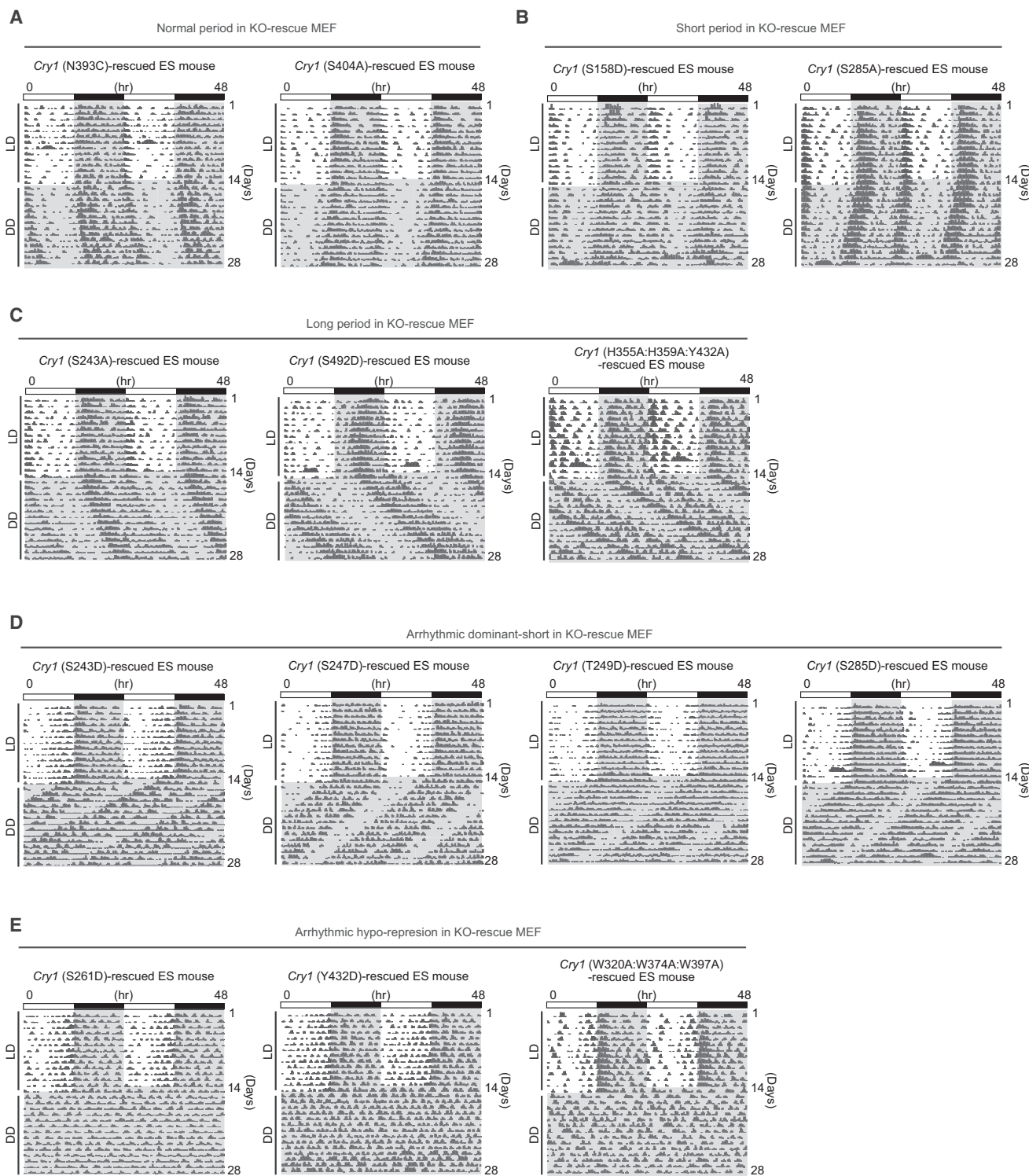


Figure 4. The Phenotype Analysis of KO-Rescue ES Mice

Representative actograms of a *Cry1*^{-/-}:*Cry2*^{-/-} mouse rescued with indicated mutant *Cry1* in anti-sense direction, exhibiting near-wild-type period length (A), shorter period length (B), longer period (C), arrhythmic dominant-short phenotype (D), or arrhythmic hypo-repression phenotype (E) in *Cry1*^{-/-}:*Cry2*^{-/-} MEF rescue experiment shown in Figure 1. All mutant CRY1-rescued ES mouse lines analyzed in this study except for mutants shown in Figures 5C–5E are shown. The period lengths and gene-targeting conditions are summarized in Table S7. See also Table S7.

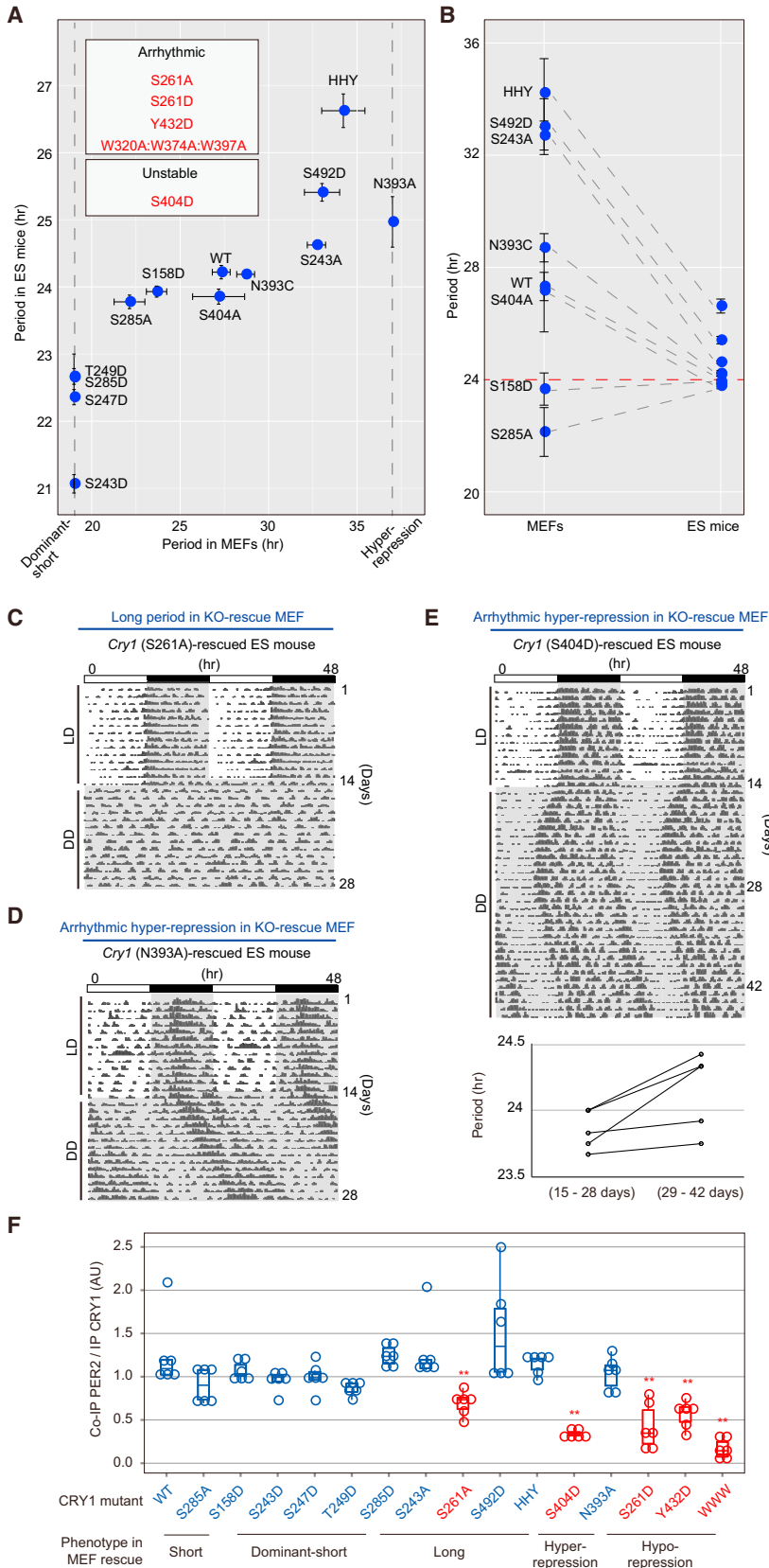


Figure 5. The Circadian Phenotype of KO-Rescue ES Mice

(A) Summary of period in behavioral rhythmicity. The representative behavioral plots are shown in Figure 4 and Figures 5B–5D. The behavioral period in constant darkness condition was calculated and shown as average \pm SD. The period (or, categories in arrhythmic mutants) of molecular oscillation recorded in rescued MEF (i.e., results shown in Figure 1D) is plotted against the period of behavioral rhythmicity in rescued mice. Mutants shown in red are arrhythmic or show unstable period in rescued mice.

(B) For each mutant that was rhythmic both in rescued MEF and rescued mice, the period lengths of MEF and mice were compared.

(C) A representative actogram of a *Cry1*^{-/-}:*Cry2*^{-/-} mouse rescued with S261A mutant CRY1.

(D) A representative actogram of a *Cry1*^{-/-}:*Cry2*^{-/-} mouse rescued with N393A mutant CRY1.

(E) Top: a representative actogram of a *Cry1*^{-/-}:*Cry2*^{-/-} mouse rescued with S404D mutant CRY1. Because the period lengths of behavioral rhythmicity are unstable in this mutant line, the recording was extended over 4 weeks in constant darkness. Bottom: the period was calculated for the first 2 weeks and the second 2 weeks of constant darkness condition for each S404D-rescued mouse.

(F) Interaction of CRY1 mutant and PER2 was quantified by co-immunoprecipitation (IP) and mass spectrometry-based quantification. Three different PER2-derived peptides were quantified in two independent experiments. Data are shown as box-and-whisker plot and individual quantified values; each circle indicates the quantified value of peptide derived from PER2 protein normalized by the amount of CRY1 protein.

***p* < 0.05; *p* > 0.1, Student's *t* test compared with WT. See also Table S7.

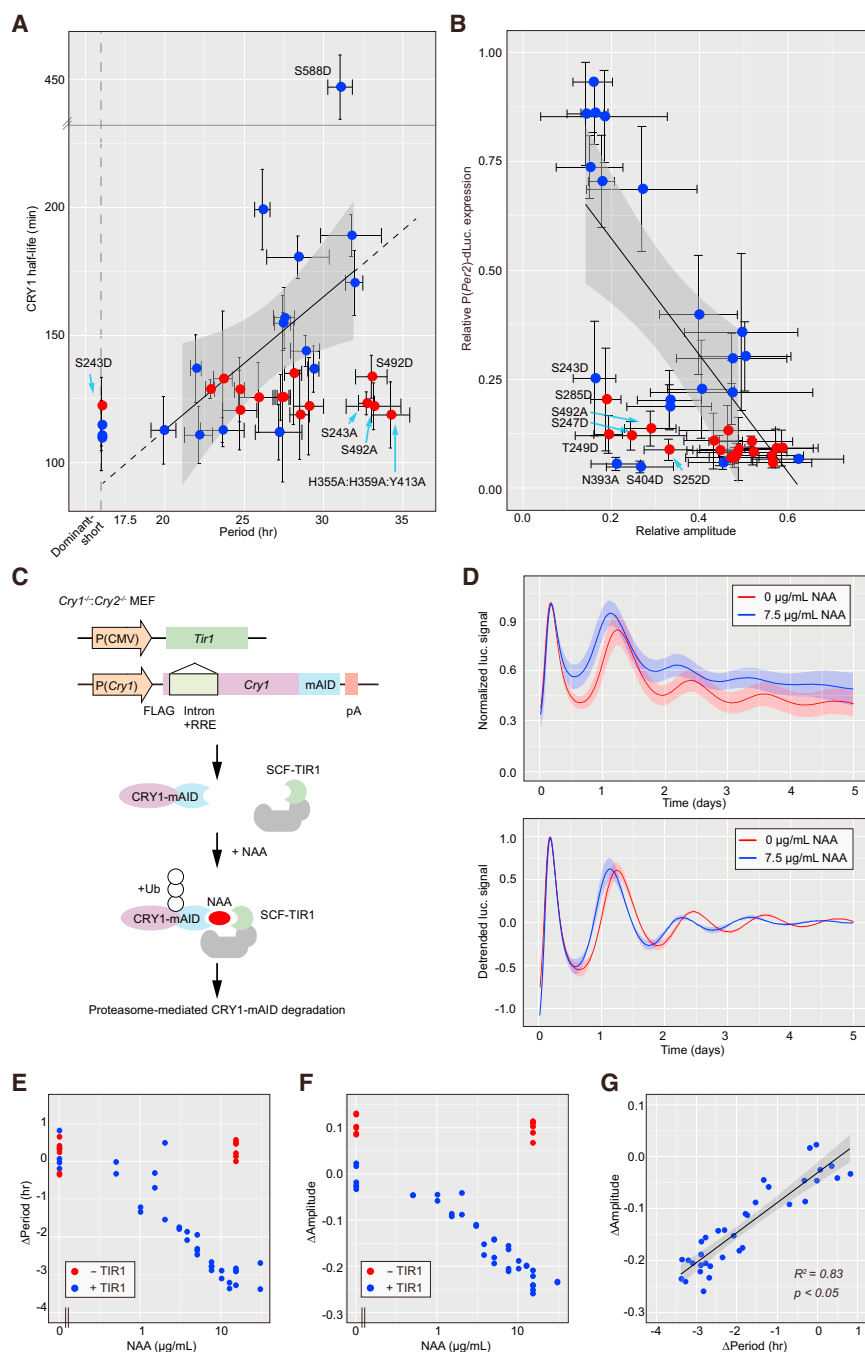


Figure 6. Causality of Increased CRY1 Turnover Rate to Circadian Period Shortening

(A) Circadian period of each mutant CRY1 in rescued MEF (data shown in Figure 1D) was plotted against protein half-life (average \pm SD). Mutants with significantly shorter or longer half-life ($p < 0.1$, Student's t test compared with wild-type) are shown in blue, and mutants with similar half-life compared with wild-type are shown in red. "Arrhythmic hyper-repression" mutants were not plotted. See Figure S4A for the half-life of each mutants and Figure S4C for the linear regression. (B) Relative amplitude of circadian rhythmicity in rescued MEF (data shown in Figure 1D) was plotted against relative activity of P(Per2)-dLuc co-transfected with each mutant CRY1 (average \pm SD). Mutants with significantly higher or lower repression activity ($p < 0.1$, Student's t test compared with wild-type) are shown in blue, and mutants with similar repression activity compared with wild-type are shown in red. See Figure S4B for the half-life of each mutants and Figure S4C for the linear regression.

(C) Scheme of the construction of CRY1-mAID system. *Tir1* was expressed under constitutive (non-circadian) promoter. A fragment of the original AID/IAA17 tag called mini-AID (mAID) (Kubota et al., 2013) was fused with the C-terminal of CRY1. AID-tagged CRY1 was expressed under the *Cry1*-rescue promoter. Addition of NAA induces the degradation of AID-tagged CRY1. Ub, ubiquitin.

(D) Circadian oscillation of rescued MEF with AID-tagged CRY1 in the presence of TIR1. The experiments were carried out as in Figure 1 except for that indicated amount of NAA was added to the medium. The upper half shows the normalized signal of P(Per2)-dLuc signal, and the lower half is the detrended oscillation signal.

(E) Changes in the oscillation period of CRY1-mAID rescued MEF. The period length of each experiment was compared with the average period of CRY1-mAID rescued MEF in the presence of TIR and 0 $\mu\text{g/mL}$ of NAA.

(F) Changes in the oscillation amplitude of CRY1-mAID rescued MEF. The relative amplitude of each experiment was compared with the average amplitude of CRY1-mAID rescued MEF in the presence of TIR and 0 $\mu\text{g/mL}$ of NAA.

(G) Correlation of amplitude reduction and period shortening by induction of CRY1-mAID degradation.

See also Figure S4.

T249D, and S285D) had decreased protein stability, if any, similar to the other short mutants. Hence, it is difficult to quantitatively explain the remarkable period shortening observed in ES mice only by decreased CRY1 protein stability.

Causality of Increased CRY1 Turnover Rate to Circadian Period Shortening

The finding of mutants that alter the circadian period with modest effect on the CRY1 stability challenges the canonical relationship between CRY1 degradation and period shortening. To ask the

causality between them, we tried to induce targeted and artificial proteolysis of CRY1 by using Auxin-induced degradation (AID) system (Figure 6C) (Kubota et al., 2013; Nishimura et al., 2009): the AID-tag is recognized by TIR1 protein, a subunit of SCF ubiquitin ligase, in the presence of auxin, leading to the proteasome-mediated degradation of AID-tagged protein in an auxin's dose-dependent manner. The tagged CRY1 successfully repressed the E-box-mediated transcription and that activity is reduced by the addition of synthetic auxin (naphthaleneacetic acid [NAA]) in a dose-dependent and TIR-dependent manner

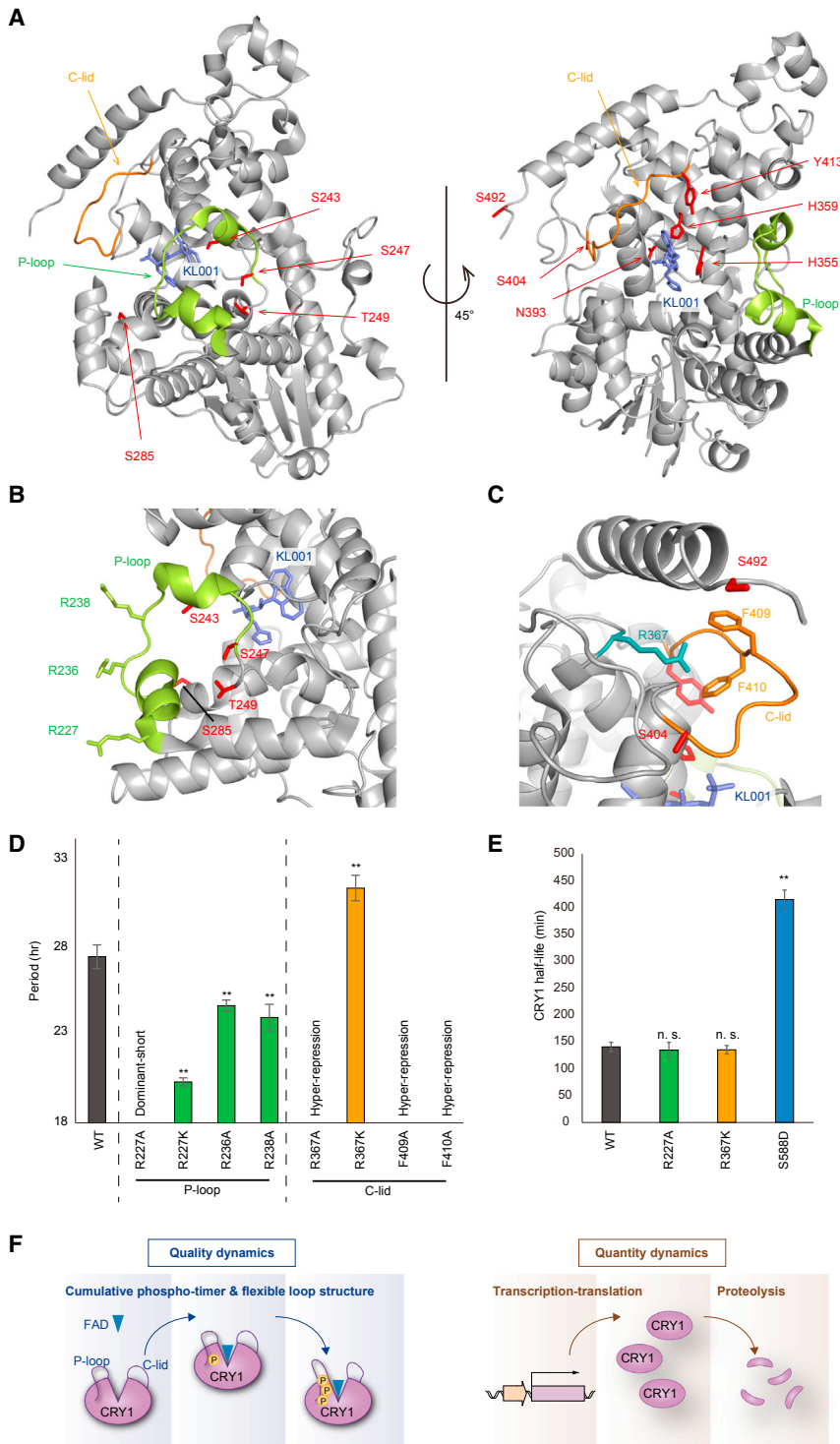


Figure 7. P Loop and C-lid as Period-Determining Domains of CRY1 Protein

(A) Crystal structure of Mm CRY2 bound to FAD analog KL001 (PDB: 4MLP) (Nangle et al., 2013). Note that S404 is not conserved in Mm CRY2 (substituted with alanine).

(B) A close-up view of the P loop and surrounding regions.

(C) A close-up view of the C-lid and surrounding regions. Two phenylalanine residues (F409, F410) on the C-lid are sterically close to an R367 residue that penetrates into the C-lid loop structure.

(D) Circadian period lengths of indicated CRY1 mutants. The arrhythmic mutants were classified based on the phenotype of NIH 3T3 overexpressed with the mutant (shown in Figure S5F). The experiments were carried out as in Figure 1.

**p < 0.05; Student's t test compared with WT. The period lengths are shown as average ± SD and summarized in Table S8.

(E) Protein half-life of indicated CRY1 mutants shown as average ± SD. The experiments were carried out as in Figure 6. **p < 0.05, n.s. p > 0.1; Student's t test compared with WT.

(F) Proteolysis-dependent and -independent circadian-period determination by CRY1. See also Table S8 and Figures S5 and S6.

decreased by the induction of CRY1 proteolysis (Figure 6F), resulting in a linear correlation between period and amplitude (Figure 6G). The result of induced CRY1 degradation suggest that the canonical relationships between circadian period and CRY1's half-life is applicable to circadian phenotype several CRY1 mutants, although such relationships cannot explain some exceptional mutants with drastic effects on the circadian period and rhythmicity.

P Loop and C-lid as Period-Determining Domains of CRY1 Protein

We then mapped the positions of such exceptional mutation on the reported CRY structures. Note that CRY2 structure bound with KL001 was used in this structural analysis because P loop structure was determined only in CRY2 but not in CRY1 (Nangle et al., 2013). Residue position number corresponding to CRY1 was used because of the consistency

(Figures S4D–S4F). Furthermore, tagged CRY1 rescued the circadian rhythmicity in the *Cry1*^{-/-}:*Cry2*^{-/-} MEF (Figure 6D). The period of rescued rhythmicity became shorter in a NAA-dose-dependent manner (Figures 6D and 6E), confirming the causal effect of CRY1 degradation on circadian period shortening. The amplitude of oscillating reporter signal was also

with our mutagenesis assay. We focused on residues that, when mutated, result in markedly long-period phenotypes (HHY, S492D, S492A, and S243A), arrhythmic dominant-short phenotypes (S243D, S247D, T249D, and S285D) or arrhythmic hyperrepression phenotypes (S404D and N393A). Figure 7A indicates that all the above-listed residues are located around

the co-factor (FAD/KL001) binding pocket of the CRY protein, especially the two loop domain called the P loop and C-lid. H355, H359, and Y413 are located near the co-factor (FAD/KL001) binding pocket and can interact with a potential co-factor. Consistently, KL001 had no detectable effect on HHY mutant (Figure S5A). Although S492 has no direct interaction with C-lid domain or co-factor binding pocket, phosphorylation of S492 residue might affect the structure of downstream, non-crystallized C-terminal domain. On the basis of these arrangement of non-canonical period-determining residues, we anticipated that the P loop and C-lid, both of which are suggested to be flexible domain (Figure S5B) (Czarna et al., 2013; Nangle et al., 2013, 2014; Schmalen et al., 2014; Xing et al., 2013), are the core domains of CRY1 in circadian-period determination. If these domains are responsible for period determination without changing CRY1 protein stability, it may be possible that structure-guided engineering of CRY1 mutation on these domain structures recapitulates proteolysis-independent period modulation.

To test this, we focused on the arginine triplet on the P loop domain (i.e., R227, R236, and R238) (Figures 7B and S5C) because the positively charged and surface-oriented arginine triplet may be involved in the interaction between CRY1 and other factors. We also focused on R367 and F409/F410 for C-lid structure because the interaction of these residues may restrict the flexibility of the C-lid (Figures 7C and S5D). As expected, mutation on each residue altered circadian oscillation of CRY1-rescued *Cry1^{-/-};**Cry2^{-/-}* MEF (Figure 7D). The alanine substitution of each arginine triplet resulted in a short-period phenotype with most drastic effect for the R227A mutation. The arrhythmic dominant-short phenotype of R227A was partially attenuated when the positively charged residue lysine substituted the position (R227K). In contrast, alanine substitution of the F409 and F410 at C-lid and the same substitution of their contact partner R367 resulted in arrhythmic hyper-repression phenotype (Figures 7D, S5E, and S5F; Table S8). When lysine substituted the R367 position, the R367K mutant had a significantly longer phenotype. We then picked up R227A and R367K mutants for P loop and C-lid domain, respectively, and investigated the protein stability of these mutants. As expected, Figure 7E shows that the protein stability of these mutants was not significantly changed compared with wild-type. The longer half-life of S588D mutant as observed in Figure 6A confirmed the robustness of this assay. The involvement of FAD-binding pocket and surrounding regions in the period determination are also supported by the result showing that cysteine residues involved in the disulfide bond at C-lid terminal (Schmalen et al., 2014) and residues mutated in *Drosophila* CRY (*cry^B*) (Stanewsky et al., 1998) are also important for the circadian-period determination in mammalian CRY1 (Figures S6B and S6C). Taken together, these data suggest that structural/electrostatic properties of P loop and C-lid are important for proteolysis-independent circadian-period determination (Figure 7F).

DISCUSSION

Multisite Phosphorylation of CRY1 Can Serve as a Cumulative Timer

The linear and additive effect of phosphorylation mutants (Figure 2) implies that CRY1 plays a role as a cumulative timer. Pre-

vious studies as well as database/algorithm-based prediction provide (Table S4) various possible kinases responsible for the phosphorylation of CRY1. The multisite phosphorylation may integrate internal information (e.g., spent time) and external information (e.g., environmental signals) and converts them into circadian-period modulation. Indeed, we identified dual phosphorylated peptide near the flexible P loop (Table S1, S243/S247). Multisite phosphorylation often occurs and regulates flexible structures or intrinsically disordered regions. This type of regulation was found in FRQ in *Neurospora* and PER in mammals (Wright and Dyson, 2015) and may be a shared design principle for the control of circadian time keeping mechanism.

The role of phosphorylation may be different depending on the target site; in our assay, S243 is the only residue, of which phosphorylation-mimetic and non-phosphorylation-mimetic mutants have opposite effect in period length, suggesting that proper level of phosphorylation on this site and/or a timely phosphorylation along with the circadian cycle is important for the circadian time keeping. There are other classes of phosphorylation site, in which only either the phosphorylation-mimetic or the non-phosphorylation-mimetic mutant had a significant effect on the circadian period (e.g., S71). This may be related to the phosphorylation level of each site. If one site is constitutively phosphorylated during the circadian cycle, then non-phosphorylation-mimetic mutation rather than phosphorylation-mimetic one would cause a severe effect. Contrary, if one site is rarely phosphorylated, then phosphorylation-mimetic mutation may cause a greater effect. For the mutants showing that both of alanine and aspartic acid substitution cause the similar effect on period length (e.g., T131), it is likely that the exact composition of side chain as well as negative charge might be important for the circadian phenotype. To validate these predictions in future studies, quantitative measurement of phosphorylation at each site, efficient detection of multi-phosphorylated peptides, and identification of responsible kinases/phosphatases will be important.

CRY1-PER2 Interaction Confers a Robust Circadian Rhythmicity in Mice

Previous study indicated that disulfide bond between C363 and C412 residues in CRY1 controls CRY1's affinity to PER2 protein, and mutation on either one of two cysteine residues increased the CRY1-PER2 interaction (Schmalen et al., 2014). However, our study showed that C363A mutation resulted in period lengthening while C412A mutation resulted in period shortening (Figure S6B). Thus, the phenotype of circadian period appears to be not matched with the phenotype of CRY1-PER2 interaction. This suggests that the phenotype of circadian period is caused by altered structure of mutated residues not simply by the breakage of disulfide bond. This result also implies that the importance of CRY1-PER2 interaction for circadian clockworks may lie in aspects other than period-determination processes. Notably, our KO-rescue ES mouse analyses revealed the role of CRY1-PER2 interaction for the robust circadian rhythmicity in vivo rather than period-determination and CRY1's repression activity (Figure 5).

Convergence of Period Length toward 24 hr in Mice

It has been reported that period variance of SCN and organism behavior is smaller than that of MEFs and dispersed SCN cells (Liu et al., 2007; Welsh et al., 2004). Our KO-rescue ES mouse analyses further revealed that period difference of CRY1 mutants observed in MEFs converged toward 24 hr in ES mice (Figure 5B). It is difficult to attribute the conversion effect to *Cry1*-driven feedback loop because we created long and short period mutants, all of which directly targeted the CRY1 molecule. Despite this, the periods of short mutants measured in MEFs were lengthened in ES mice, and the periods of long mutants measured in MEFs were shortened in ES mice. Thus, it is suggested that the molecular/cellular nature of convergence-to-24 hr-effect, not just the reduction of variance, is not related to *Cry1* gene. Interestingly, Ono et al. demonstrated that circadian oscillation can be observed in *Cry1^{-/-}:Cry2^{-/-}* mice in a limited developmental condition (Ono et al., 2013), suggesting the presence of *Cry1/2*-independent circadian oscillator. Our CRY1 mutagenesis assay revealed that CRY1-PER2 interaction is particularly important for robust rhythmicity in mice. Phosphorylation of PER2 by CKI δ/ϵ have several intriguing features such as temperature-compensation (Isojima et al., 2009) and reciprocal regulation of CKI ϵ (Qin et al., 2015) that have a potential to create phosphorylation-based autonomous oscillators (Jolley et al., 2012). These features imply that part of the mammalian circadian rhythmicity might rely upon *Per2*-driven oscillators. Therefore, one possible perspective is that *Per2*-driven oscillator couples with *Cry1*-driven oscillator to confer a near 24-hr rhythmicity.

Circadian-Period Determination by CRY1 Degradation-Dependent and -Independent Mechanisms

Our study suggests that the P loop and C-lid are responsible for the protein-stability-independent period determination. Previous studies revealed that C-lid forms an interface between CRY1/2 and PER2 (Figure S6D) (Nangle et al., 2014; Schmalen et al., 2014) or FBXL3 (Xing et al., 2013), and the C-lid structure is affected by the binding of these proteins (Figure S6E). P loop is not directly involved in the interface between PER2 or FBXL3, but it may affect the interaction through creating the co-factor binding pocket. Indeed, residues of CRY1 affecting the interaction with PER2 identified in this study locate around co-factor binding pocket (hence surrounding C-lid or P loop) (Figure S6D). However, our study suggests that the period-determination mechanism can be independent from CRY1 stability that is regulated through FBXL3 and PER2 competition. Thus, it is also possible that the C-lid and P loop may regulate circadian period through the interaction with other proteins because CRY proteins function in a 2-MDa complex composed of tens of proteins (Brown et al., 2005; Duong et al., 2011; Kim et al., 2015). In summary, this study proposes that mammalian circadian period is controlled not only by the turnover rate of CRY1, a behavior determined by the *quantity* of molecules, but also by the *quality* of each molecule characterized by the structure of flexible loops and phosphorylation status.

EXPERIMENTAL PROCEDURES

Detailed information was described in [Supplemental Experimental Procedures](#).

Circadian Reporter Assay using *Cry1^{-/-}:Cry2^{-/-}* MEFs and NIH 3T3 Cells

Real-time monitoring of circadian reporter using culture cells was performed as previously described (Ukai-Tadenuma et al., 2011). In brief, cells were transfected with pGL3-P(*Per2*)-dLuc reporter plasmid and each *Cry1* gene expression vector. The cells were synchronized by adding forskolin to the medium. The bioluminescence was monitored at 30°C.

Generation of ES Mice and Behavior Analysis

An ESC clone was injected into 8-cell-stage ICR embryos to generate ES mice (Kiyonari et al., 2010). C57BL/6 wild-type mice (9 weeks old), *Cry1^{-/-}:Cry2^{-/-}* mice (12 weeks old), ES mice (7-10 weeks old), F1 animals of WT rescue (AS) (10 weeks old) were entrained to a light-12 hr:dark-12 hr cycle for at least 2 weeks and then the locomotor activity was collected in the light-dark condition for 1-2 weeks and then in the dark-dark (DD) condition for another 2-4 weeks. All experimental procedures and housing conditions involving animals and their care were approved the Institutional Animal Care and Use Committee of RIKEN Kobe Branch.

Analysis of CRY1 Half-Life and Transcription-Repression Activity

Vector construct that express *Cry1::luciferase* under the non-circadian CMV promoter (pMU2-*Cry1::luciferase*) was transfected to *Cry1^{-/-}:Cry2^{-/-}* MEFs. Luciferase signal was chased after the addition of 400 μ g/mL of cycloheximide to the medium. Transcription repression assay was performed as described previously (Khan et al., 2012).

SUPPLEMENTAL INFORMATION

Supplemental Information includes Supplemental Experimental Procedures, six figures, and eight tables and can be found with this article online at <http://dx.doi.org/10.1016/j.molcel.2016.11.022>.

AUTHOR CONTRIBUTIONS

H.R.U., K.L.O., H.U., and E.A.S. designed the study. K.L.O. performed most of the cellular/biochemical experiments, and data analysis. H.U., E.A.S., N.K., T.A., and H.K. established a KO-rescue ES mouse method. E.A.S. and J.H. performed animal experiments. R.N. and K.M. performed phospho-peptide quantification. M.T.K. and K.L.O. established the AID system in circadian assay. H.R.U., K.L.O., H.U., and E.A.S. wrote the manuscript. All authors discussed the results and commented on the manuscript.

ACKNOWLEDGMENTS

We thank all the lab members at RIKEN QBIC and the University of Tokyo, in particular, Dr. Masahiro Hayashi and Dr. Genshiro A. Sunagawa for helping with animal experiments; Chikako Imai, Ayumi Kishimoto, Satoko Morino, and Marie Muramatsu for their effort to maintain ESCs; Junko Garçon, Kaori Yamanaka, and Shino Hirahara for their effort with the production of ES mice; Maki Ukai-Tadenuma for helping with the cellular assay; Dr. Rikuhiko G. Yamada for assisting mice behavior analysis; and Yoshiki Nagashima for supporting analyses with a mass spectrometer. We also thank the LARGE, RIKEN CLST for housing the mice. We thank Dr. Arthur Millius for critical reading and valuable comments on the manuscript. We are grateful to Dr. Eisuke Nishida for providing pcDNA3-*Myc-mPer2* and Dr. Haruhiko Takisawa for sharing unpublished data. This work was supported by a grant from AMED-CREST (H.R.U.), CREST (H.R.U.), Brain/MINDS (H.R.U.), Basic Science and Platform Technology Program for Innovative Biological Medicine (H.R.U.), the Cell Innovation Program (H.R.U.), KAKENHI Grants-in-Aid from JSPS (Scientific Research S, 25221004, H.R.U.; Scientific Research on Innovative Areas, 23115006, H.R.U.; Young Scientists B, 25830146, K.L.O.; Challenging Exploratory Research, 16K14653, K.L.O.; Young Scientists A, 15H05650, E.A.S.), the strategic programs for R&D of RIKEN (H.R.U.), an intramural Grant-in-Aid from the RIKEN QBIC (H.R.U.), grants from Takeda Science Foundation

(H.R.U. and E.A.S.), the RIKEN Special Postdoctoral Research Program (E.A.S.), a Grant-in-Aid by PRESTO from JST (E.A.S.), a Grant-in-Aid from the Japan Foundation for Applied Enzymology (E.A.S.), and a grant of the Brain Sciences Project of the Center for Novel Science Initiatives of the National Institutes of Natural Sciences (BS281004, E.A.S.).

Received: September 14, 2016

Revised: October 24, 2016

Accepted: November 15, 2016

Published: December 22, 2016

REFERENCES

- Antoch, M.P., Song, E.J., Chang, A.M., Vitaterna, M.H., Zhao, Y., Wilsbacher, L.D., Sangoram, A.M., King, D.P., Pinto, L.H., and Takahashi, J.S. (1997). Functional identification of the mouse circadian Clock gene by transgenic BAC rescue. *Cell* 89, 655–667.
- Brown, S.A., Ripperger, J., Kadener, S., Fleury-Olela, F., Vilbois, F., Rosbash, M., and Schibler, U. (2005). PERIOD1-associated proteins modulate the negative limb of the mammalian circadian oscillator. *Science* 308, 693–696.
- Busino, L., Bassermann, F., Maiolica, A., Lee, C., Nolan, P.M., Godinho, S.I., Draetta, G.F., and Pagano, M. (2007). SCFFbx3 controls the oscillation of the circadian clock by directing the degradation of cryptochrome proteins. *Science* 316, 900–904.
- Czarna, A., Berndt, A., Singh, H.R., Grudziecki, A., Ladurner, A.G., Timinsky, G., Kramer, A., and Wolf, E. (2013). Structures of *Drosophila* cryptochrome and mouse cryptochrome1 provide insight into circadian function. *Cell* 153, 1394–1405.
- Duong, H.A., Robles, M.S., Knutti, D., and Weitz, C.J. (2011). A molecular mechanism for circadian clock negative feedback. *Science* 332, 1436–1439.
- Forger, D.B. (2011). Signal processing in cellular clocks. *Proc. Natl. Acad. Sci. USA* 108, 4281–4285.
- Gao, P., Yoo, S.H., Lee, K.J., Rosensweig, C., Takahashi, J.S., Chen, B.P., and Green, C.B. (2013). Phosphorylation of the cryptochrome 1 C-terminal tail regulates circadian period length. *J. Biol. Chem.* 288, 35277–35286.
- Godinho, S.I., Maywood, E.S., Shaw, L., Tucci, V., Barnard, A.R., Busino, L., Pagano, M., Kendall, R., Quwallid, M.M., Romero, M.R., et al. (2007). The after-hours mutant reveals a role for Fbx3 in determining mammalian circadian period. *Science* 316, 897–900.
- Hirota, T., Lee, J.W., St John, P.C., Sawa, M., Iwaisako, K., Noguchi, T., Pongsawakul, P.Y., Sonntag, T., Welsh, D.K., Brenner, D.A., et al. (2012). Identification of small molecule activators of cryptochrome. *Science* 337, 1094–1097.
- Isojima, Y., Nakajima, M., Ukai, H., Fujishima, H., Yamada, R.G., Masamoto, K.H., Kiuchi, R., Ishida, M., Ukai-Tadenuma, M., Minami, Y., et al. (2009). CK1 ϵ / δ -dependent phosphorylation is a temperature-insensitive, period-determining process in the mammalian circadian clock. *Proc. Natl. Acad. Sci. USA* 106, 15744–15749.
- Jolley, C.C., Ode, K.L., and Ueda, H.R. (2012). A design principle for a post-translational biochemical oscillator. *Cell Rep.* 2, 938–950.
- Khan, S.K., Xu, H., Ukai-Tadenuma, M., Burton, B., Wang, Y., Ueda, H.R., and Liu, A.C. (2012). Identification of a novel cryptochrome differentiating domain required for feedback repression in circadian clock function. *J. Biol. Chem.* 287, 25917–25926.
- Kim, J.Y., Kwak, P.B., Gebert, M., Duong, H.A., and Weitz, C.J. (2015). Purification and analysis of PERIOD protein complexes of the mammalian circadian clock. *Methods Enzymol.* 551, 197–210.
- Kiyonari, H., Kaneko, M., Abe, S., and Aizawa, S. (2010). Three inhibitors of FGF receptor, ERK, and GSK3 establishes germline-competent embryonic stem cells of C57BL/6N mouse strain with high efficiency and stability. *Genesis* 48, 317–327.
- Kubota, T., Nishimura, K., Kanemaki, M.T., and Donaldson, A.D. (2013). The Elg1 replication factor C-like complex functions in PCNA unloading during DNA replication. *Mol. Cell* 50, 273–280.
- Lamia, K.A., Sachdeva, U.M., DiTacchio, L., Williams, E.C., Alvarez, J.G., Egan, D.F., Vasquez, D.S., Juguilon, H., Panda, S., Shaw, R.J., et al. (2009). AMPK regulates the circadian clock by cryptochrome phosphorylation and degradation. *Science* 326, 437–440.
- Larrondo, L.F., Olivares-Yañez, C., Baker, C.L., Loros, J.J., and Dunlap, J.C. (2015). Circadian rhythms. Decoupling circadian clock protein turnover from circadian period determination. *Science* 347, 1257277.
- Liu, A.C., Welsh, D.K., Ko, C.H., Tran, H.G., Zhang, E.E., Priest, A.A., Buhr, E.D., Singer, O., Meeker, K., Verma, I.M., et al. (2007). Intercellular coupling confers robustness against mutations in the SCN circadian clock network. *Cell* 129, 605–616.
- Mohawk, J.A., Green, C.B., and Takahashi, J.S. (2012). Central and peripheral circadian clocks in mammals. *Annu. Rev. Neurosci.* 35, 445–462.
- Nakajima, M., Imai, K., Ito, H., Nishiwaki, T., Murayama, Y., Iwasaki, H., Oyama, T., and Kondo, T. (2005). Reconstitution of circadian oscillation of cyanobacterial KaiC phosphorylation in vitro. *Science* 308, 414–415.
- Nangle, S., Xing, W., and Zheng, N. (2013). Crystal structure of mammalian cryptochrome in complex with a small molecule competitor of its ubiquitin ligase. *Cell Res.* 23, 1417–1419.
- Nangle, S.N., Rosensweig, C., Koike, N., Tei, H., Takahashi, J.S., Green, C.B., and Zheng, N. (2014). Molecular assembly of the period-cryptochrome circadian transcriptional repressor complex. *eLife* 3, e03674.
- Nishimura, K., Fukagawa, T., Takisawa, H., Kakimoto, T., and Kanemaki, M. (2009). An auxin-based degron system for the rapid depletion of proteins in nonplant cells. *Nat. Methods* 6, 917–922.
- Ono, D., Honma, S., and Honma, K. (2013). Cryptochromes are critical for the development of coherent circadian rhythms in the mouse suprachiasmatic nucleus. *Nat. Commun.* 4, 1666.
- Oshima, T., Yamanaka, I., Kumar, A., Yamaguchi, J., Nishiwaki-Ohkawa, T., Muto, K., Kawamura, R., Hirota, T., Yagita, K., Irle, S., et al. (2015). C-H activation generates period-shortening molecules that target cryptochrome in the mammalian circadian clock. *Angew. Chem. Int. Ed. Engl.* 54, 7193–7197.
- Ozturk, N., Song, S.H., Ozgür, S., Selby, C.P., Morrison, L., Partch, C., Zhong, D., and Sancar, A. (2007). Structure and function of animal cryptochromes. *Cold Spring Harb. Symp. Quant. Biol.* 72, 119–131.
- Pearlman, S.M., Serber, Z., and Ferrell, J.E., Jr. (2011). A mechanism for the evolution of phosphorylation sites. *Cell* 147, 934–946.
- Qin, X., Mori, T., Zhang, Y., and Johnson, C.H. (2015). PER2 differentially regulates clock phosphorylation versus transcription by reciprocal switching of CK1 ϵ activity. *J. Biol. Rhythms* 30, 206–216.
- Sanada, K., Harada, Y., Sakai, M., Todo, T., and Fukada, Y. (2004). Serine phosphorylation of mCRY1 and mCRY2 by mitogen-activated protein kinase. *Genes Cells* 9, 697–708.
- Sancar, A. (2004). Regulation of the mammalian circadian clock by cryptochrome. *J. Biol. Chem.* 279, 34079–34082.
- Schmalen, I., Reischl, S., Wallach, T., Klemz, R., Grudziecki, A., Prabu, J.R., Benda, C., Kramer, A., and Wolf, E. (2014). Interaction of circadian clock proteins CRY1 and PER2 is modulated by zinc binding and disulfide bond formation. *Cell* 157, 1203–1215.
- Siepkka, S.M., Yoo, S.H., Park, J., Song, W., Kumar, V., Hu, Y., Lee, C., and Takahashi, J.S. (2007). Circadian mutant Overtime reveals F-box protein FBXL3 regulation of cryptochrome and period gene expression. *Cell* 129, 1011–1023.
- Stanewsky, R., Kaneko, M., Emery, P., Beretta, B., Wager-Smith, K., Kay, S.A., Rosbash, M., and Hall, J.C. (1998). The cryb mutation identifies cryptochrome as a circadian photoreceptor in *Drosophila*. *Cell* 95, 681–692.

- Sung, Y.H., Baek, I.J., Kim, D.H., Jeon, J., Lee, J., Lee, K., Jeong, D., Kim, J.S., and Lee, H.W. (2013). Knockout mice created by TALEN-mediated gene targeting. *Nat. Biotechnol.* *31*, 23–24.
- Ukai-Tadenuma, M., Yamada, R.G., Xu, H., Ripperger, J.A., Liu, A.C., and Ueda, H.R. (2011). Delay in feedback repression by cryptochrome 1 is required for circadian clock function. *Cell* *144*, 268–281.
- van der Horst, G.T., Muijtjens, M., Kobayashi, K., Takano, R., Kanno, S., Takao, M., de Wit, J., Verkerk, A., Eker, A.P., van Leenen, D., et al. (1999). Mammalian Cry1 and Cry2 are essential for maintenance of circadian rhythms. *Nature* *398*, 627–630.
- Welsh, D.K., Yoo, S.H., Liu, A.C., Takahashi, J.S., and Kay, S.A. (2004). Bioluminescence imaging of individual fibroblasts reveals persistent, independently phased circadian rhythms of clock gene expression. *Curr. Biol.* *14*, 2289–2295.
- Wright, P.E., and Dyson, H.J. (2015). Intrinsically disordered proteins in cellular signalling and regulation. *Nat. Rev. Mol. Cell Biol.* *16*, 18–29.
- Xing, W., Busino, L., Hinds, T.R., Marionni, S.T., Saifee, N.H., Bush, M.F., Pagano, M., and Zheng, N. (2013). SCF(FBXL3) ubiquitin ligase targets cryptochromes at their cofactor pocket. *Nature* *496*, 64–68.

Molecular Cell, Volume 65

Supplemental Information

Knockout-Rescue Embryonic Stem Cell-Derived

Mouse Reveals Circadian-Period Control

by Quality and Quantity of CRY1

Koji L. Ode, Hideki Ukai, Etsuo A. Susaki, Ryohei Narumi, Katsuhiko Matsumoto, Junko Hara, Naoshi Koide, Takaya Abe, Masato T. Kanemaki, Hiroshi Kiyonari, and Hiroki R. Ueda

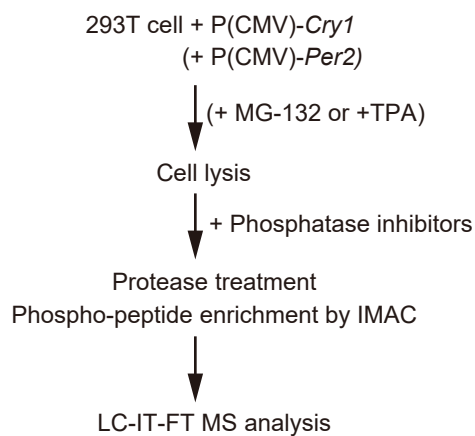
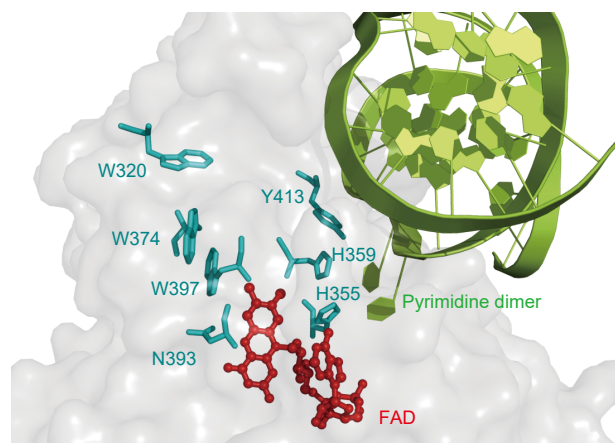
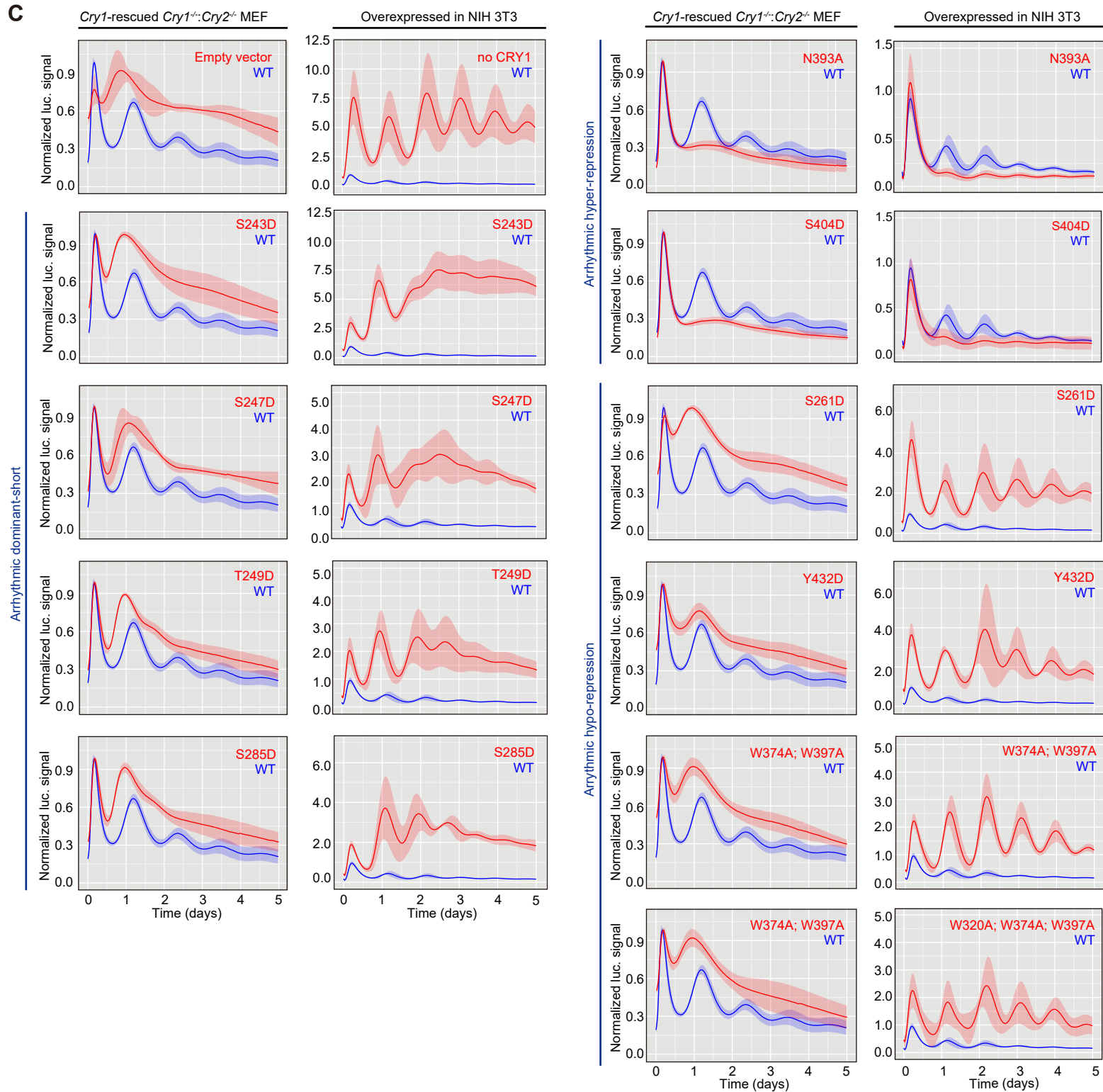
A**B****C**

Figure S1: Ode *et al.*

Figure S1 related to Figure 1. Phosphorylation sites and conserved canonical electron-transfer residues in CRY1.

(A) Scheme for the LC-MS based identification of phosphorylation residues in CRY1. CRY1 was over-expressed under the CMV promoter in 293T cells. Assay condition and identified peptide list are summarized in **Table S1** and **Supplemental Experimental Procedures**. TPA: 12-O-tetradecanoylphorbol 13-acetate. IMAC: immobilized metal affinity chromatography.

(B) A canonical electron-transfer pathway in 6-4 photolyase of *Drosophila melanogaster* (PDB 3CVY) (Maul et al., 2008). Green; damaged DNA substrate. Red; Co-factor FAD. Cyan; residues involved in a canonical-transfer pathway. During the photoexcitation of flavin chromophore at 6-4 photolyase, tryptophan triplet (W320, W374, and W397 as corresponding residues in mice CRY1) and histidine/tyrosine triplet (H355, H359, and Y413 in mice CRY1) are thought to mediate electron transfer to excite the chromophore and damaged DNA substrate (Aubert et al., 2000; Hitomi et al., 2001; Maul et al., 2008; Sadeghian et al., 2010). The photoactivated chromophore may be stabilized through the interaction with asparagine residue (N393 in mice CRY1) (Hitomi et al., 2009; Li et al., 2010; Liu et al., 2011). Note that all residues are conserved in mouse CRY1, and the amino acid numbers are shown based on mouse CRY1.

(C) Examples of arrhythmic cellular phenotype in CRY1-rescued *Cry1^{-/-}:Cry2^{-/-}* MEF (left). The arrhythmic phenotype was further classified based on the phenotype when the same CRY1-rescue and P(*Per2*)-d*Luc* plasmids were co-transfected into NIH 3T3 cells (right). For the experiments using NIH 3T3 cells in this and the other figures, the luciferase signal was normalized such that the maximum value of wild-type CRY1's time course data in each experiment is to be one, and shown as average (solid line) ± SD (shade) (n > 4, taken from at least two independent experiments).

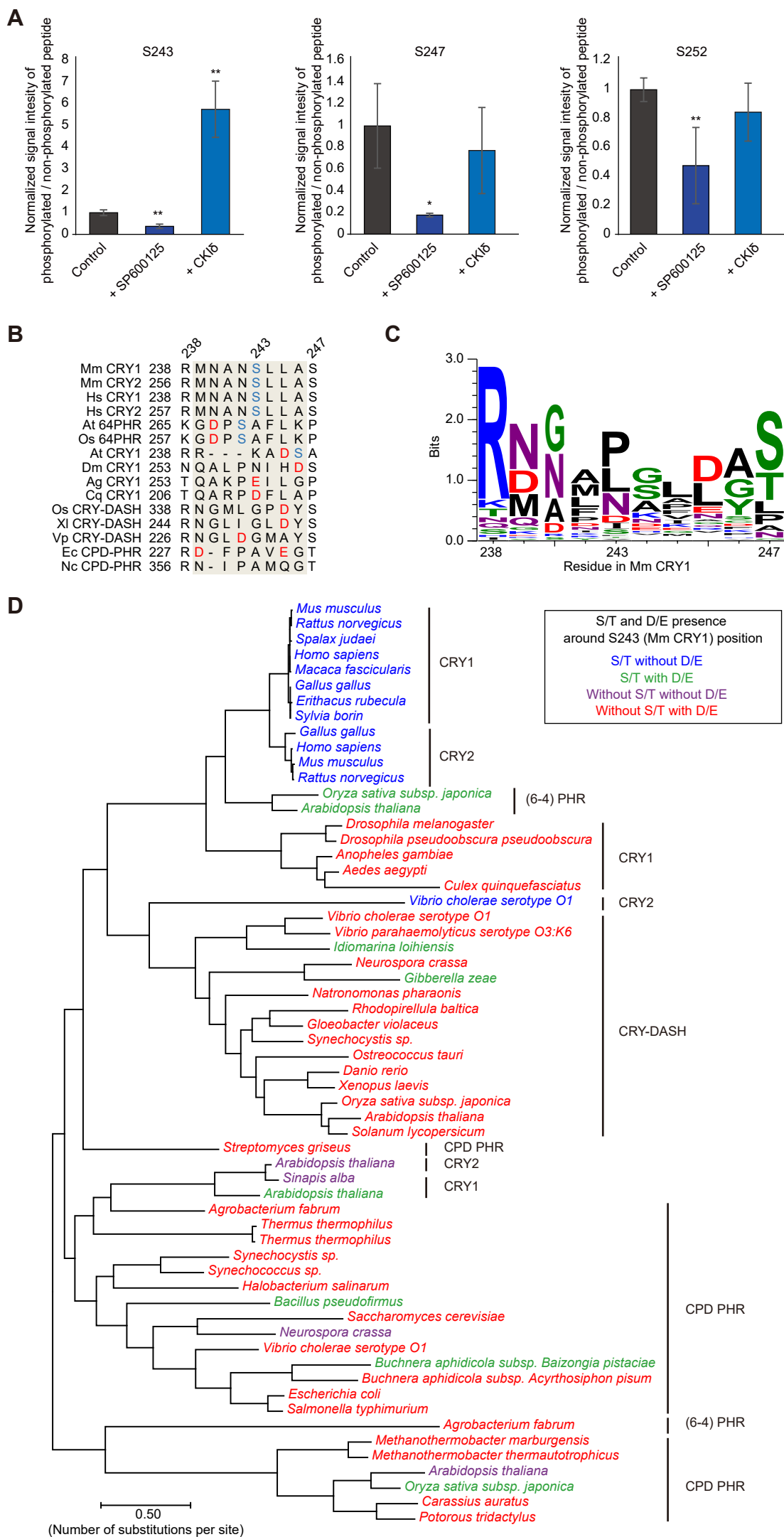


Figure S2: Ode et al.

Figure S2 related to Figure 2. Evolutional conservation of S243 and neighboring phosphorylation residues in CRY1.

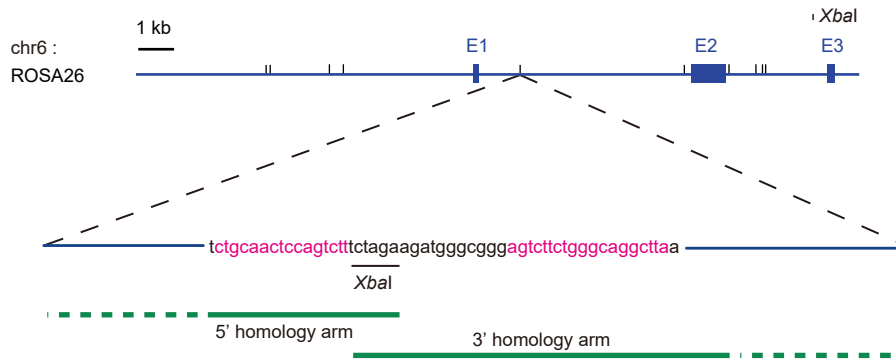
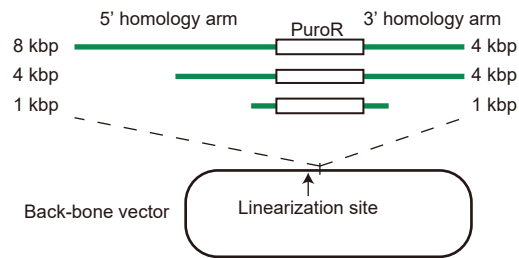
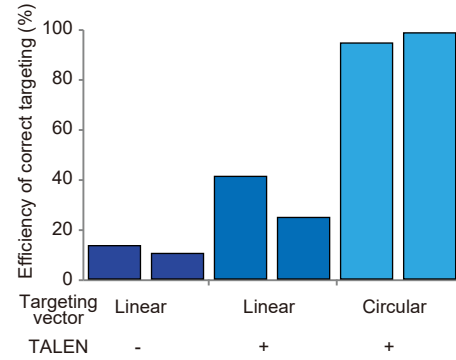
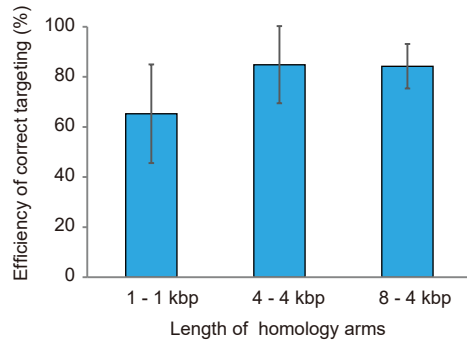
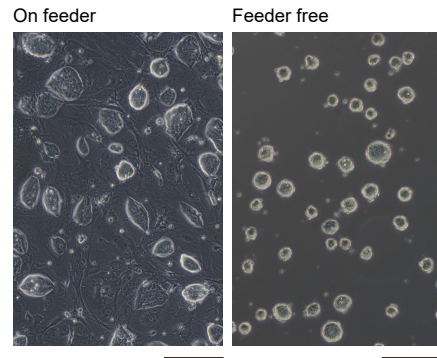
(A) Quantification of phosphorylated peptides derived from CRY1. CRY1 were overexpressed in 293T cells in the absence or presence of 100 μ M SP600125, or co-overexpression of CKI δ . The ratio of peptide with phosphorylation at indicated residues to unphosphorylated peptide was quantified by triple quadrupole mass spectrometer using isotopically-labelled synthetic peptides as internal controls. The ratio of phosphorylated S243 to non-phosphorylated one was decreased by the addition of potent CKI δ/ϵ inhibitor SP600125 (Isojima et al., 2009) and increased by the co-expression of CKI δ . SP600125 treatment also decreased the phosphorylation level of S247 and T249, residues adjacent to S243 and responsible for arrhythmic dominant-short phenotype although the effects of CKI δ co-expression were not significant. The quantified values are shown as average \pm SD (n = 4). ** $p < 0.05$, * $p < 0.1$, n.s.; $p > 0.1$; Student's t-test compared with "Control". Quantified sequences and quantification method are summarized in **Supplemental Experimental Procedures** and **Table S5**.

(B) Sequence alignment of S243 surrounding region of cryptochrome super family. The alignment was conducted against all protein listed in (C). Arginine/lysine (R/K) at R238 position and serine/threonine (S/T) at S247 position are well conserved across many phyla. The area between these two conserved residues (shaded), S/T residue are colored in blue and aspartic acid/glutamic acid are colored in red. Mm: *Mus musculus*. Hs: *Homo sapiens*. At: *Arabidopsis thaliana*. Os: *Oryza sativa*. At: *Arabidopsis thaliana*. Dm: *Drosophila melanogaster*. Ag: *Anopheles gambiae*. Cq: *Culex quinquefasciatus*. Xl: *Xenopus laevis*. Vp: *Vibrio parahaemolyticus*. Ec: *Escherichia coli*. Nc: *Neurospora crassa*.

(C) Amino acid conservation of S243 surrounding region displayed in the Sequence Logo. S243 is located in the middle of evolutionally well-conserved R/K at R238 position of CRY1 and also well-conserved S/T at S247 position of CRY1. Between

these well-conserved residues, negatively-charged aspartic acid and glutamic acid (D/E) often appear.

(D) Phylogenetic tree of the *cryptochrome* superfamily. For each protein, residues aligned within the 239 - 246 position in Mm CRY1 (brown shaded in (B)) were analysed. Blue; at least one S or T residue is involved in the 239 - 246 region, and no D, or E is involved in the region. Green; at least one S or T residue and at least one D, or E residue are involved in the region. Purple; the region does not involve any S, T, D, and E residues. Red; at least one D, or E residue is involved in the 239 - 246 region, and no S or T is involved in the region. The phylogenetic tree shows that mammalian cryptochromes have S but no D/E within the 239 - 246 position in Mm CRY1. On the other hand, most of the other cryptochrome superfamily proteins have D/E but no S/T within this area. If the role of phosphorylation for regulating the protein function largely relies on its negative charge rather than specific surface structure of specific residue position, then phosphorylation within local area similarly plays a role regardless of the exact position (Nash et al., 2001; Orlicky et al., 2003). Therefore, in the view of electrostatic condition, phosphorylation of S243 might mimic the protein surface of other cryptochrome superfamily proteins.

A**B****C****D****E****F**

Line of ESC	Culture condition	No. of embryos	No. of pups born	No. of 100% chimeras	Ratio of 100% chimeras to pups born
#1	On feeder	96	17	16	94.1%
#2	On feeder	97	14	11	78.6%
#3	Feeder free	83	10	8	80.0%
#4	Feeder free	96	21	17	81.0%
#5	Feeder free	83	19	16	84.2%
#6	Feeder free	75	30	15	50.0%

Figure S3: Ode *et al.*

Figure S3 related to Figure 3. TALEN-based high-efficient establishment of knock-in ES mouse

(A) Schematic of the TALEN-targeting site at the ROSA26. The nucleotide sequence of the target site containing the TALEN recognition sites (labelled in magenta) is shown. XbaI-digestion site sequence is underlined. Corresponding regions for 3'-terminal of 5' homology arm and 5'-terminal of 3' homology arm of targeting vector are indicated as green lines.

(B) Schematic of three different targeting vector constructs for assays shown in C and D. Each vector includes 5' and 3' homology arm (green lines) of the different length each. Arm length is given in kilo base pairs. Gene for targeting is shown as a white box. The back-bone vector is illustrated as a loop. A linearization site at the flanking site of 5' homology arm is indicated by an arrow. Puromycin-resistant gene was knocked-into the ROSA26 locus so that the efficiency of targeting was quantified as the number of survived colonies in the presence of puromycin.

(C) Efficiency of correct targeting of linearized/circular targeting vector. Linearized/circular targeting vector were transfected with/without TALEN. Length of 5' and 3' homology arm of targeting vector is 4 kbp. Targeted integration at the ROSA26 were assayed by PCR for over twelve puromycin-resistant colonies (each experiment contains 2 samples; n = 2). TALEN-based targeting on the ROSA26 locus significantly increased the efficiency of genome editing up to almost 90% with circular vector as reported in zinc finger nuclease based targeting (Orlando et al., 2010).

(D) Efficiency of correct targeting of three different targeting vectors. Circular targeting vectors (illustrated in (B)) were transfected with TALEN. Targeted integration at the ROSA26 assayed by PCR for over 12 puromycin-resistant colonies for each experiments. Average \pm SEM (error bar) of three independent experiments are shown. We concluded that the optimal length was from 4 kbp to 8 kbp. Thus, in the KO-rescue of ES mice experiments, we chose 8 kbp length for the 5' homology arm of ROSA26

locus and 4 kbp for the 3' homology arm of ROSA26 locus as reported previously (Abe et al., 2011).

(E) Three-days cultured HK3i ESCs (Kiyonari et al., 2010) under with (left) or without (right) feeder cell condition. Scale bar, 200 μ m.

(F) Efficiency of contribution for chimeric embryos of ESCs cultured under with or without feeder cells condition. HK3i ESCs were injected into 8-cell embryos after ten-passages. The efficiency of contribution was judged with a coat color. That feeder-free culture condition can gain ESCs that kept comparable efficiency to contribute chimeric embryos with ESCs in classical culture condition with feeder cells.

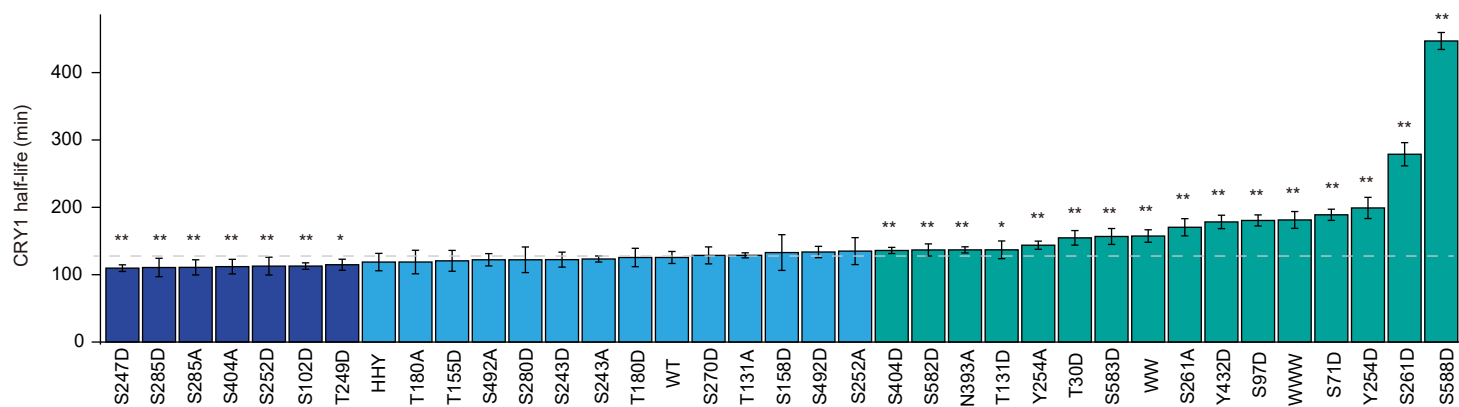
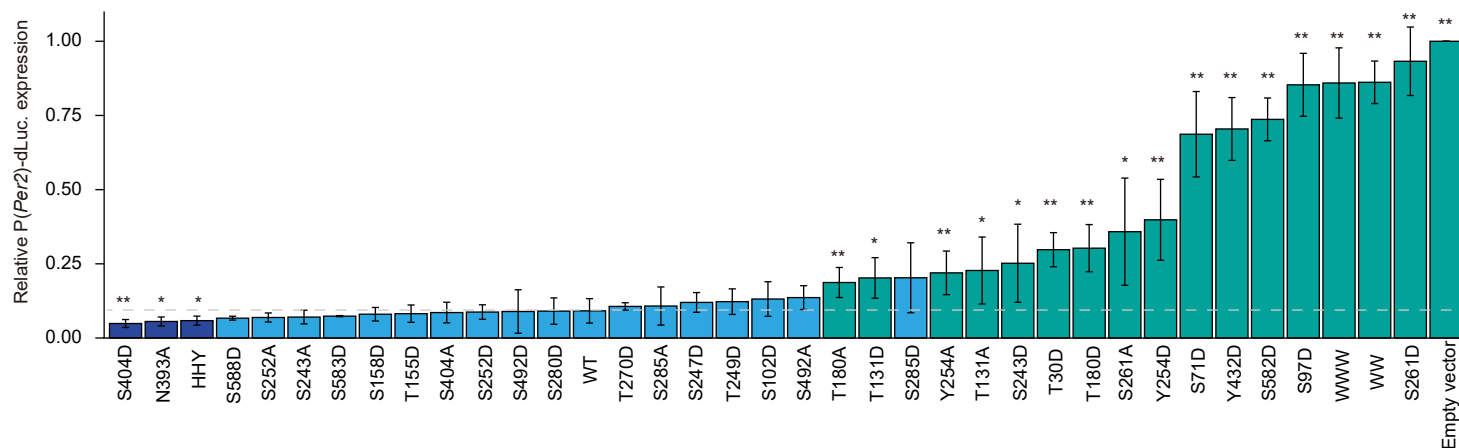
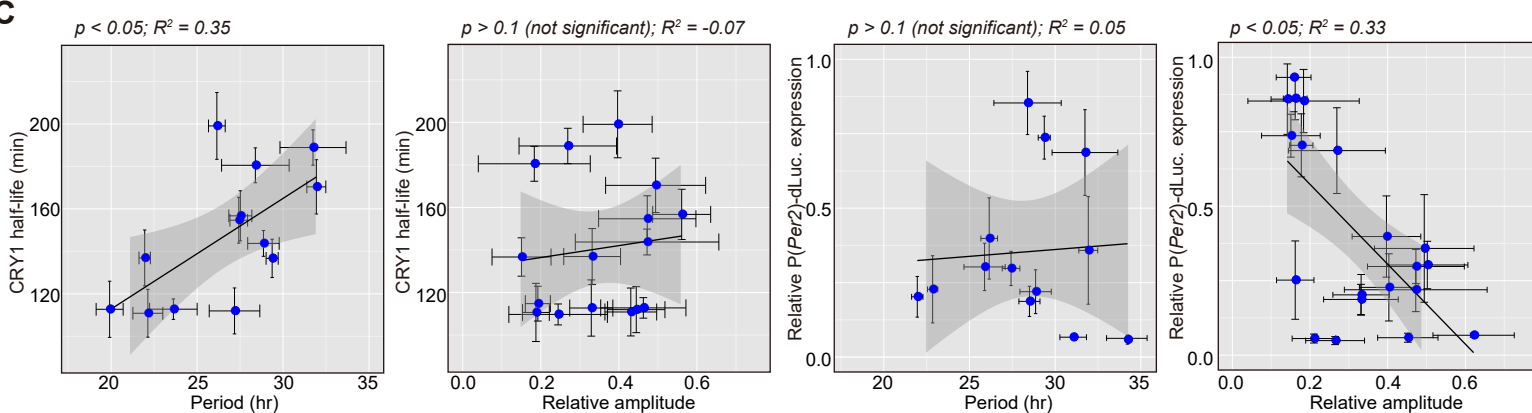
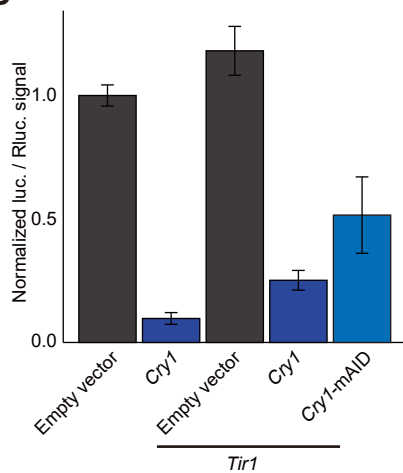
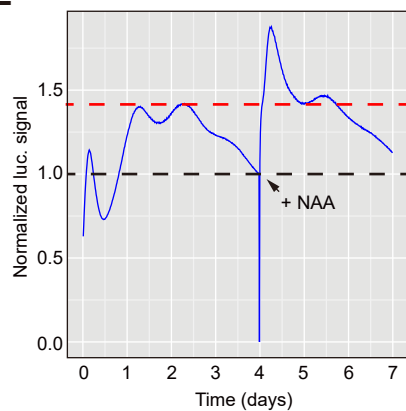
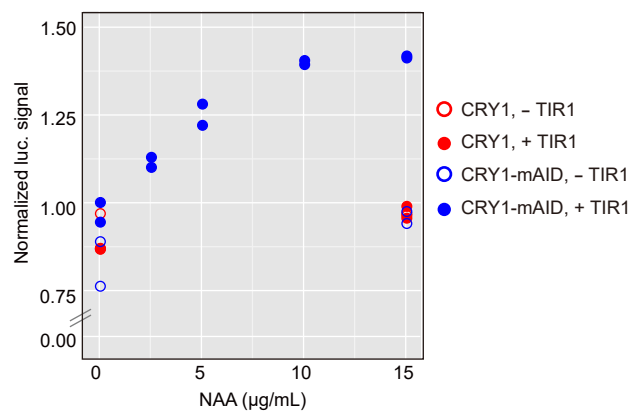
A**B****C****D****E****F**Figure S4: Ode *et al.*

Figure S4 related to Figure 6. Correlation between CRY1 half-life and circadian period length.

(A) Protein half-life of indicated mutant/wild-type CRY1 were plotted. A vector plasmid expressing CRY1::luciferase fusion protein was transfected into *Cry1^{-/-}:Cry2^{-/-}* MEFs. The luciferase signal was then chased upon addition of 400 $\mu\text{g/mL}$ cycloheximide. Data are shown as average \pm SD ($n = 4$). ** $p < 0.05$, * $p < 0.1$, n.s.; $p > 0.1$; Student's t-test compared with WT. Dark-blue bars; mutants with significantly reduced protein half-life. Light-blue bars; mutants with protein half-life similar to that of wild type. Green bars; mutants with significantly increased protein half-life. WW; W374A:W397A, WWW; W320A:W374A:W397A, HHY; H355A:H359A:Y413A.

(B) E-box repression activity of indicated mutant/wild-type CRY1 are plotted. A vector plasmid expressing CRY1, P(*Per2*)-dLuc reporter, and a plasmid expressing Renilla luciferase (RLuc) were co-transfected to *Cry1^{-/-}:Cry2^{-/-}* MEFs. The signal of luciferase normalized to the signal of RLuc are plotted. Data are shown as average \pm SD ($n = 4\text{--}8$). ** $p < 0.05$, * $p < 0.1$, n.s.; $p > 0.1$; Student's t-test compared with WT. Dark-blue bars; mutants with significantly increased transcription-repression activity. Light-blue bars; mutants with transcription-repression activity similar to that of wild type. Green bars; mutants with significantly increased transcription-repression activity.

(C) Simple regression analysis for protein half-life (A), repression activity (B), circadian oscillation period and amplitude (shown in **Figure 1D**). For CRY1 mutants that have significant change in their half-life, the correlation of CRY1 half-life with circadian period or circadian amplitude observed in the assay of KO-rescue MEFs was calculated. Similarly, for CRY1 mutants with significantly altered transcription-repression activity, the correlation of CRY1 repression activity with circadian period or circadian amplitude was calculated. Note that arrhythmic mutants were excluded from the analysis including oscillation period because the exact period lengths were undetermined, and S588D mutant was excluded from the analysis including protein half-life because this mutant shows exceptionally long half-life, though including the

S588D for this correlation analysis does not change our conclusion (i.e. significant correlation between period and half-life). Solid line: regression line with two-sided 95% confidence interval. *P*-value of F-test and adjusted R-squared value are shown in upper right.

(D) E-box repression activity of AID-tagged CRY1. The experiment was carried out same as in (B) but using a plasmid expressing CRY1-mAID, and a plasmid expressing TIR1 for the indicated assay conditions.

(E) Baseline response of P(*Per2*)-*dLuc* reporter signal to the addition of NAA. The reporter plasmid, plasmid expressing CRY1-mAID and TIR1 were transfected into *Cry1^{-/-}:Cry2^{-/-}* MEFs as indicated in **Figure 6C**. To monitor the baseline level of luciferase reporter, forskolin stimulation was not applied in this experiment (i.e. the cells were circadian-asynchronous). Four days after the medium exchange, NAA was added; and then signal at the first trough after NAA addition was quantified (red dotted line) and normalized to the signal at the NAA addition (black dotted line). The plot shows a representative result with the addition of 15 µg/mL NAA.

(F) The normalized baseline signal as analysed in (E) in various conditions. The baseline signal responded to NAA in a dose-dependent manner in the presence of TIR1 and AID-tagged CRY1.

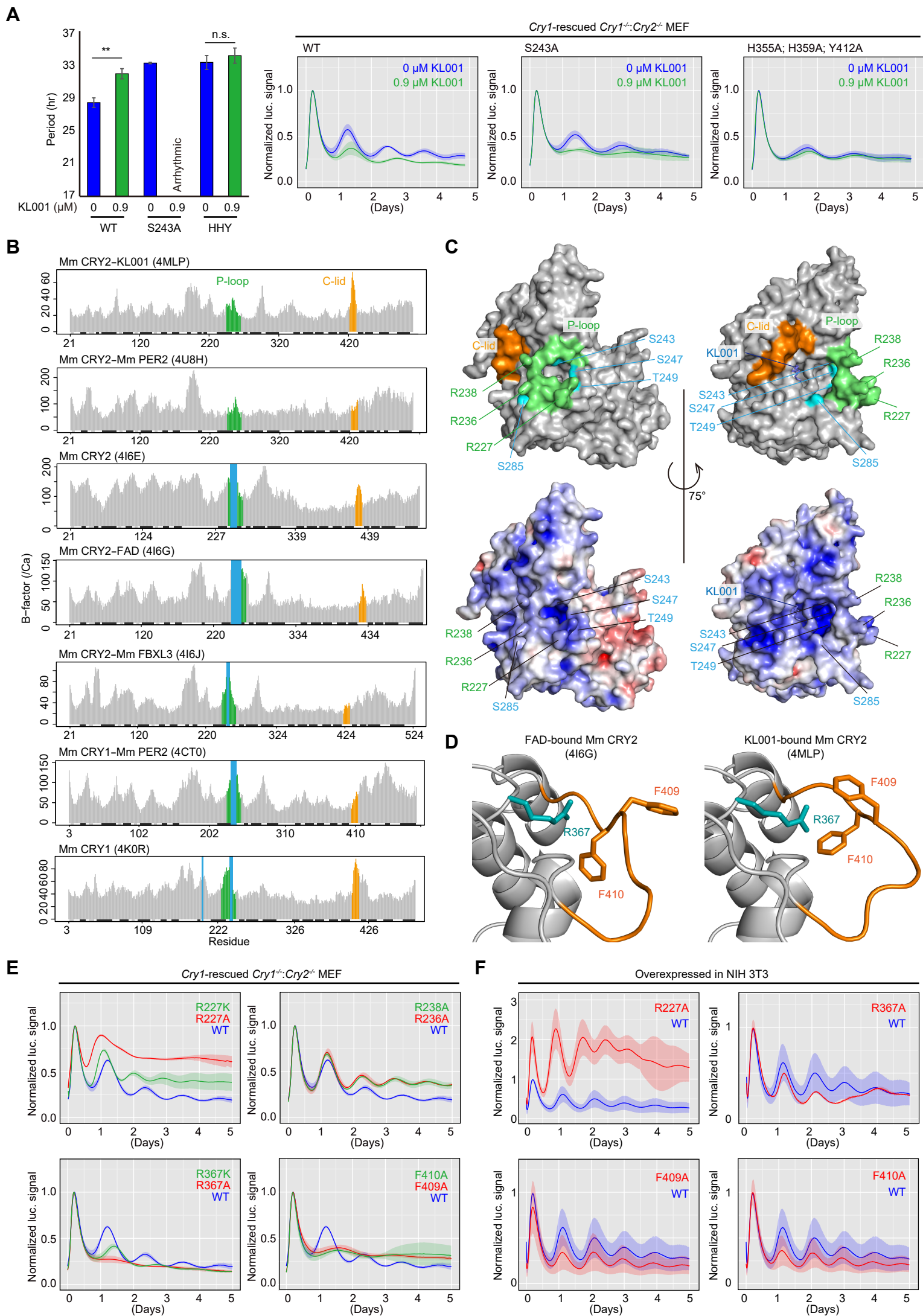


Figure S5: Ode et al.

Figure S5 related to Figure 7. Effect on circadian period by the modulation of residues around co-factor binding pocket.

(A) The HHY mutant CRY1 has reduced sensitivity to KL001. Circadian rhythmicity of *Cry1^{-/-}:Cry2^{-/-}* MEF rescued by indicated wild-type/mutant CRY1 was monitored in the presence of indicated concentration of KL001. KL001 significantly affected circadian period of wild type and long-period S243A mutant. In contrast, KL001 had no detectable effect on HHY mutant. Quantified period plot (left) and circadian oscillation (right) were shown as average \pm SD ($n = 4$). ** $p < 0.05$, n.s. $p > 0.1$; Student's t-test compared with the period in the absence of KL001.

(B) The B-factor (temperature factor) of alpha carbon atoms in published mammalian CRY1 crystal structures (Czarna et al., 2013; Nangle et al., 2013; Nangle et al., 2014; Schmalen et al., 2014; Xing et al., 2013). Green bars indicate p-loop (R227 – S247 in Mm CRY1; R245 – S265 in Mm CRY2) and orange bars indicate C-lid (S404 – Y413 in Mm CRY1; A422 – Y431 in Mm CRY2). The B-factor of these loops are higher than other domains of CRY protein, or the structure of P-loop domain was partially not determined (shaded in blue) in several structures.

(C) Upper half represents Mm CRY2 structure colored based on p-loop (green), C-lid (orange) and phosphorylated residues responsible for the arrhythmic dominant-short phenotype (cyan). Arginine triplet on p-loop are also indicated. Bottom half represents the Mm CRY2 surface colored based on electrostatic potential in a linear color ramp from -6.0 kT (red) to 6.0 kT (blue). The protein surface is based on Mm CRY2-KL001 structure PDB: 4MLP (Nangle et al., 2013). Note that all amino acid residue number are based on Mm CRY1 in this and following panels.

(D) Structural alteration of C-lid upon co-factor binding. C-lid (orange), R367 residue (cyan) and their up/down stream helices are shown. Compared with the FAD bound form of Mm CRY2 (PDB: 4I6G) (Xing et al., 2013), F409 and F410 residues on c-loop change their position to be close to R367 residue upon KL001 binding (PDB: 4MLP) (Nangle et al., 2013).

(E) Circadian rhythmicity of wild-type/mutant CRY1 rescued *Cry1^{-/-}:Cry2^{-/-}* MEF. The quantified periods are shown in **Figure 7D**. The experiments were carried out same as in **Figure 1**. Note that the data for wild type on each panel are identical.

(F) The arrhythmic mutants were expressed in NIH 3T3 for the classification of arrhythmic dominant-short, hyper-repression, and hypo-repression phenotypes. The experiments were carried out same as in **Figure 1**. R227A was classified as arrhythmic dominant-short, whereas the other three mutants were classified as arrhythmic hyper-repression. The classified results were also shown in **Figure 7D**. Note that the data for wild type on each panel are identical.

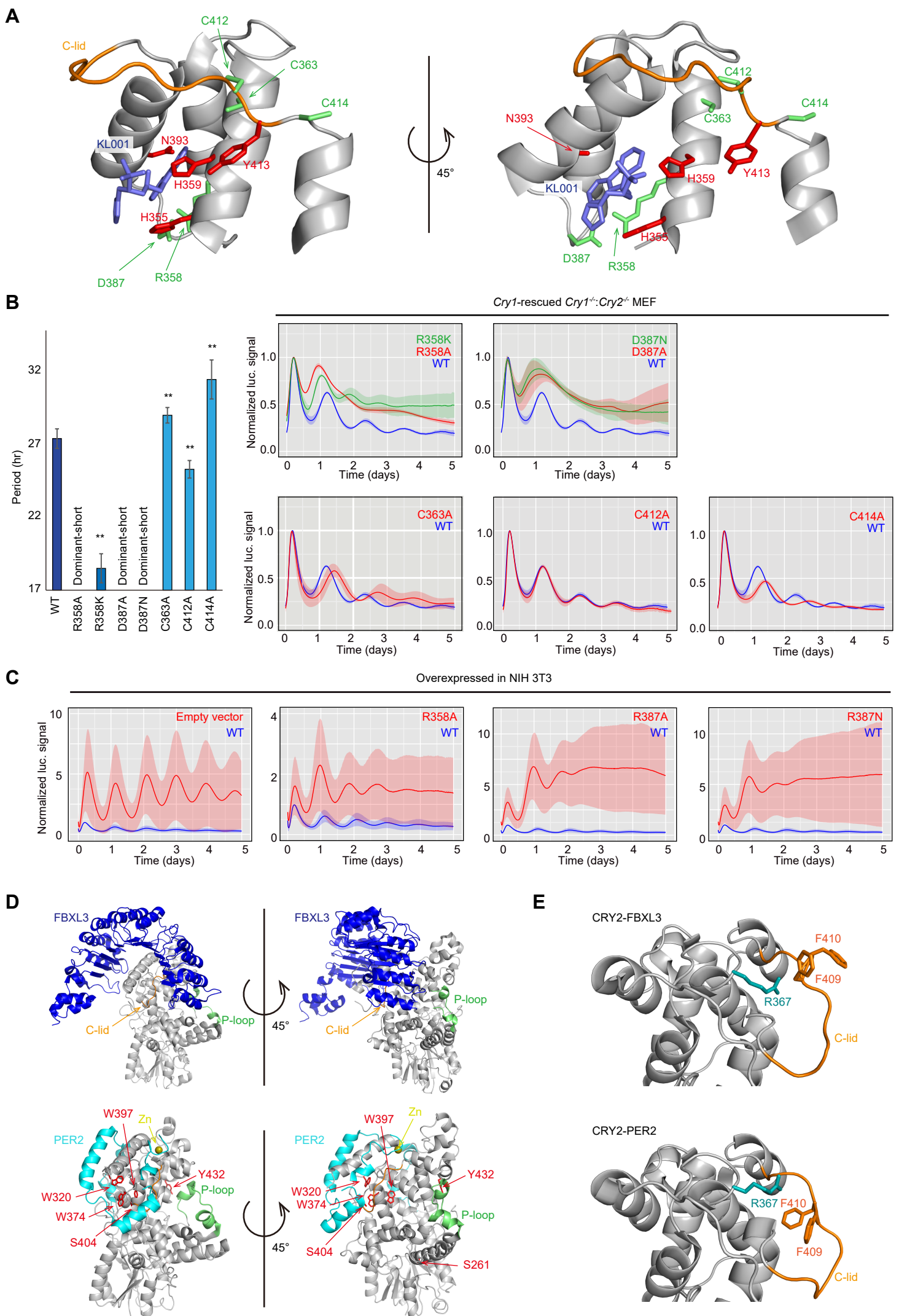


Figure S6: Ode *et al.*

Figure S6 related to Figure 7. Disulfide bond and hydrogen bond regulating the circadian period length.

(A) A close-up view of FAD-binding pocket. The salt-bridge between R358 and D387 has been shown to affect the repression of BMAL1/CLOCK activity in Mm CRY1 (Hitomi et al., 2009) and photoreception activity of *Drosophila* CRY (*cry^b*) (Stanewsky et al., 1998). The disulfide bridge between C363 and C412, and zinc binding of C414 have been shown to affect Mm CRY1-Mm PER2 interaction (Schmalen et al., 2014).

(B) Circadian rhythmicity of *Cry1^{-/-}:Cry2^{-/-}* MEF rescued by indicated wild-type/mutant CRY1. The quantified periods are shown in bar plot on the left. Panels on the right indicate circadian oscillation of rescued cells. The experiments were carried out same as in **Figure 1**. Note that the data for wild type is the same as shown in **Figure S5E**. Arrhythmic mutants were classified based on the experiments shown in (C). ** $p < 0.05$; Student's t-test compared with "WT". The period lengths are shown as average \pm SD (n = 4) and summarized in **Table S8**.

(C) The arrhythmic mutants shown in (B) were expressed in NIH 3T3 for the classification of arrhythmic dominant-short, hyper-repression, and hypo-repression phenotypes. The experiments were carried out same as in **Figure 1**. R358A, D387A, and D387N were classified as arrhythmic dominant-short. Note that the data for wild type is the same as shown in **Figure S5F**.

(D) Crystal structure of Mm CRY2 in complex with FBXL3 (PDB 4I6J) (Xing et al., 2013). and Mm CRY2 in complex with PER2 (PDB 4U8H) (Nangle et al., 2014). In the CRY2-PER2 complex, residues important for the CRY1-PER2 interaction found in **Figure 5F** are shown.

(E) A close-up view of the C-lid and surrounding regions of CRY2 in complex with FBXL3 (PDB 4I6J) or PER2 (PDB 4U8H).

LIST OF SUPPLEMENTAL TABLES

Table S1 related to Figure 1:

Phosphorylated amino acid residues in CRY1

Table S2 related to Figure 1:

Circadian period and amplitude of CRY1 mutants

Table S3 related to Figure 2:

Circadian period of CRY1 double mutants

Table S4 related to Figures 2 and S2:

Prediction of kinases responsible for analyzed phosphorylation sites in CRY1

Table S5 related to Figures 2 and S2:

SRM method for the quantification of phospho-CRY1 peptides

Table S6 related to Figure 3:

Primers for ESC screening and genome integrity check

Table S7 related to Figures 3-5:

Circadian phenotype of *Cry1* (mutant)-rescued ES mouse

Table S8 related to Figures 7 and S6:

Period of CRY1 mutants around the P-loop, C-lid, and co-factor binding pocket

SUPPLEMENTAL EXPERIMENTAL PROCEDURES

Plasmid construction

Cry1, *Per2*, and *CKI δ* used in this study were subcloned in the pMU2 vector (Ukai et al., 2007) as described previously (Narumi et al., 2016) and expressed under the CMV promoter as a FLAG-tag fusion in their N terminus (pMU2-*Cry1*, pMU2-*Per2*, and pMU2-*CKI δ*). pMU2-*Cry1::luciferase* was constructed by inserting the luciferase sequence of pGL3-basic (Promega) into the C-terminus of *Cry1*. A circadian reporter plasmid pGL3-P(*Per2*)-dLuc was constructed as described previously (Sato et al., 2006). The expression vector for codon-optimized *OsTir1* (*Oryza sativa*) was constructed based on pAID1.2-N vector (Kubota et al., 2013) by removing the IRES and AID-tag-MCS sequences from the plasmid: the pAID1.2-N was digested by using restriction enzymes BamHI and PvuI. The product was treated with T4 DNA polymerase for creating blunt ends and self-ligated to obtain pAID1.2str-P(CMV)-*OsTir1*.

For the vector of *Cry1*-rescue experiment, pMU2-P(*Cry1*)-FLAG-(*Cry1* intron 336)-*Cry1* vectors used in the original study (Ukai-Tadenuma et al., 2011) was slightly modified to enhance the efficiency of splicing at intronic RRE (i.e. *Cry1* intron 336). To this end, the sequence of (*Cry1* intron 336) was designed to be flanked by the donor and acceptor of a chimeric intron derived from pCMV-TNT (Promega), which is composed of 5'-donor site from the first intron of the human β -globin gene and the branch and 3'-acceptor site from the intron of an immunoglobulin gene heavy chain variable region (Bothwell et al., 1981). First, a fragment flanked by two *Afl*III sites in the pMU2-MCS (Ukai et al., 2007) vector was removed. Second, the chimeric intron of pCMV-TNT was amplified with PCR with primers harboring *I-Sce*I or *PI-Psp*I sites (primers: 5'-ATCGATAAGCTTGATAATTACCCTGTTATCCCTAATAAGTTGGTCGTGAGGCAC-3' and 5'-CTGCAGGAATTCGATACCCATAATACCCATAATAGCTGTTTGCCAAGAGCTGTAAT

TGAACTGGG-3') and cloned into *EcoRV* site of pBluescript vector. Then, inverted PCR fragment of this vector (primers: 5'-TAGGTGCCTATCAGAAACGCA-3' and 5'-TTGGTCTTACTGACATCCACT-3') was ligated with the *Cry1* intron 336 fragment (WT or R1,2 mutation) amplified from pMU2-P(*Cry1*)-FLAG-(*Cry1* intron 336)-Luc/*Cry1* vectors (PCR primers: 5'-TTATGACACAGTGTAGAAACTATG-3' and 5'-ACCTTTTACTACTATAAAAACGTACATG-3'). Finally, P(*Cry1*) and *Cry1* coding sequences (from pMU2-P(*Cry1*)-FLAG-(*Cry1* intron 336)-*Cry1*), P(SV40) (from pGL3-basic, Promega), and the complete *Cry1* intron (5' donor - *Cry1* intron 336 - 3' acceptor) were ligated into *KpnI/HindIII* sites, *PI-PspI/PI-SceI* sites, *KpnI/HindIII* sites and *I-SceI/PI-PspI* sites of the modified pMU2-MCS vector, respectively. The final composition of the *Cry1* rescue constructs were as follow: P(*Cry1*) or P(SV40) - leader sequence (from pCMV-TNT) - ATG - FLAG - intron (WT or R1,2 mutation) - *Cry1* (WT) - SV40 late poly(A) (from pCMV-TNT). These plasmids were then named as pMU2-P(*Cry1*)-FLAG-I/RRE-*Cry1* or pMU2-P(SV40)-FLAG-I/RRE(Mut)-*Cry1*, respectively.

Site-directed mutagenesis with circular PCR followed by self-ligation of blunt-end product was performed using Mighty Cloning Reagent Set (Blunt End) (Takara bio. inc., Japan). pMU2-*Cry1*, pMU2-*Cry1::luciferase*, and pMU2-P(*Cry1*)-FLAG-I/RRE-*Cry1* were used for the template plasmids of mutagenesis. AID-tagged *Cry1* vector was constructed by inserting the 66-132 a.a. sequence of AID tag (from pAID1.2-N) into the C-terminus of *Cry1* of pMU2-P(*Cry1*)-FLAG-I/RRE-*Cry1*, and called pMU2-P(*Cry1*)-FLAG-I/RRE-*Cry1*-mAID.

Targeting vectors of ROSA26 locus were prepared as follows: pENTR-1A (Invitrogen) with Puro-resistance gene cassette (pPGK-PuroR-poly A: PuroR) flanked by FRT sequences was prepared by the insertion of PuroR at the *EcoRV* site (for sense direction) or at the *BamHI-KpnI* site (for antisense direction) of the vector. Then, the *Cry1* rescue cassettes (cut with *MluI* from the pMU2-P(*Cry1*)-FLAG-I/RRE-*Cry1* vector) were cloned into the pENTR-1A-PuroR vector at the *BamHI-NotI* site (for sense direction) or *NotI-KpnI* site (for antisense direction). The resulting expression vectors

(pENTR-1A_attL1-*Cry1* cassette-PuroR-attL2 for sense or pENTR-1A_attL1-reversed [*Cry1* cassette-PuroR]-attL2 for antisense direction) were then mixed with the ROSA26 targeting vector, which contains the Reading Frame Cassette B from the Gateway Conversion System (Invitrogen) at the blunted *KpnI* and *AscI* sites, to perform the LR recombination reaction using the Gateway system (Abe et al., 2011; Susaki et al., 2014). Plasmids for a series of mutated *Cry1* were constructed by swapping the *Cry1* coding sequence between pENTR-1A_attL1-reversed [*Cry1* cassette-PuroR]-attL2 and pMU2-P(*Cry1*)-FLAG-I/RRE-*Cry1* (mutant) using *EcoRI* and *NotI*.

Targeting vectors for comparison of the effect of the arm-length of the targeting vector to the targeting efficiency, illustrated in **Figure S3B**, were constructed as follows: 3' homology arms (4 kbp and 1 kbp) were amplified by PCR with forward primers (5'-GGCTCGATCCCTCGAGTCTAGAAGATGGGCGGGAGTCTT-3') and reverse primer (5'-CGGGAATTCGATGATATCCTCTATAGGTAGGGTTACTAGGTCA-3' or 5'-CGGGAATTCGATGATATCAGTAAGCAGTAATCAATACCATGTGG-3') and inserted into the *XhoI* and *EcoRV* digested back-bone vector, pTVCI3 (Tainaka et al., 2014), by using In-Fusion HD Cloning Kit (Clontech Laboratories, Inc. A Takara Bio Company). 5' homology arms (8 kbp, 4 kbp and 1 kbp) were amplified by PCR with forward primers (5'-TAGGGATAACAGGGTAATATAGCTGGGATTACAAGCAGCACACACA-3', 5'-TAGGGATAACAGGGTAATATAGATTAAGATGGAGGAATTCATGTCAC-3' or 5'-TAGGGATAACAGGGTAATATAGGTACGAGTCGTGACGCTGGAAG-3') and reverse primer (5'-GCGGAGAAAGAGGTAATGAAATGGTCTAGAAAGACTGGAGTTGCAGATC-3'). Then those products of 1st PCR for 5' homology arms were amplified with primers (5'-GCAGTTACGCTAGGGATAACAGGGTAATATAG-3' and 5'-GATCATCTATGTCCGGTGCGGAGAAAGAGGTAATGAAATGG-3') and inserted into the *I-SceI* and *PI-SceI* digested pTVCI3-Rarm by using In-Fusion HD Cloning Kit.

The Puromycin resistance gene cassette (P(PGK)-Puro^R-polyA) was inserted into *I-CeuI* and *PI-PspI* digested pTVCl3-LRarm.

Identification of phosphorylation sites in CRY1

Cry1 was expressed in 293T cells as previously described with several modifications (Narumi et al., 2016). At 24 hr before transfection, 293T cells were plated at 10⁶ cells per 90-mm dishes. A total of 12 µg of pMU2-*Cry1*, or a mixture of 6 µg pMU2-*Cry1* and pMU2-*Per2* was transfected to the 293T cells on a 90-mm dish. After 68 hr, cells were treated with 10 µM MG-132 or 20 nM TPA at indicated condition in **Table S1**. Four hr after the addition of the reagents, cells were collected by 0.25% trypsin–EDTA (Life Technologies) treatment. The cell pellets were lysed in 1 mL PTS buffer (12 mM sodium deoxycholate, 12 mM sodium N-lauroylsarcosinate, 50 mM NH₄HCO₃) containing Phosphatase Inhibitor Cocktail (Nacalai tesque) followed by extensive sonication. The cell lysates were then flash-frozen in liquid nitrogen and stored at -80°C. For the immunoprecipitation sample, cells were collected 72 hr after the transfection and cell pellets were lysed in 1 mL M-PER solution (Thermo Fisher Scientific) containing Phosphatase Inhibitor Cocktail (Nacalai tesque) followed by extensive sonication. The lysate was mixed with 50 µL of anti-FLAG M2 agarose beads (Sigma) by rotating for 4 hr at 4°C. The beads were rinsed with 1 mL M-PER solution three times and then incubated with 0.1 mL of 0.1 M glycine-HCl (pH 3.5) for 10 min. After the gentle centrifugation, the supernatant (IP sample) was collected and mixed with 250 µL of modified PTS buffer.

Cell lysates or IP samples were enzymatically digested according to a phase-transfer surfactant (PTS) protocol (Masuda et al., 2008). The IP sample was reduced (10 mM dithiothreitol at RT for 30 min) and alkylated (50 mM 2-iodoacetamide at RT for 30 min), and then it was diluted to 5 folds by adding 50 mM NH₄HCO₃ solution, followed by the digestion with 1 µg Lysyl Endopeptidase (LysC; Wako Pure Chemical Industries, Osaka, Japan). The samples were incubated for overnight at RT. The

sample was further digested with 1 μg trypsin for 6 hr at RT. After the digestion, an equal volume of ethyl acetate was added to the sample, which was acidified with 0.5% TFA and well mixed to transfer the detergents into an organic phase. The sample was then centrifuged at 10,000 x g for 10 min at room temperature, and an aqueous phase containing peptides was collected and dried with SpeedVac (Thermo Fisher Scientific). The dried peptides were solubilized in 100 μL of 2% acetonitrile and 0.1% TFA, and applied to Fe-IMAC (Immobilized Metal Ion Affinity Chromatography) according to the previous report (Narumi and Tomonaga, 2016) to enrich the phosphopeptides.

The LC-MS analyses were performed by data-dependent MS/MS with a IT-FT mass spectrometer (Orbitrap velocity mass spectrometer, Thermo Fisher Scientific) equipped with an HPLC system containing a nano HPLC equipment (Advance UHPLC, Bruker Daltonics) and an HTC-PAL autosampler (CTC Analytics) with a trap column (0.3 x 5 mm, L-column, ODS, Chemicals Evaluation and Research Institute, Japan). An analytical sample solubilized in 5 μL of 2% acetonitrile and 0.1% TFA was loaded to the LC-MS system to be separated by a gradient using mobile phases A (0.5% acetic acid) and B (0.5% acetic acid and 80% acetonitrile) at a flow rate 200 nL/min (Cell lysate; 5% to 35% B in 190 min, 35% to 95% B in 1 min, 95% B for 1 min, 95% to 5% B in 1 min and 5% B for 7 min. IP sample; 5% to 40% B in 40 min, 40% to 95% B in 2 min, 95% to 5% B in 1 min and 5% B for 16 min) with a home-made capillary column (length of 200 mm and inner diameter of 100 μm) packed with 3 μm C18 resin (L-column2, Chemicals Evaluation and Research Institute, Japan). The eluted peptides were electrosprayed (1.8-2.3 kV) and introduced into the MS equipment (positive ion mode, data-dependent MS/MS). The obtained raw data was subjected to database search with MASCOT (Matrix Science) algorithm running on Proteome Discoverer (Thermo Fisher Scientific).

Circadian reporter assay using *Cry1*^{-/-}:*Cry2*^{-/-} MEF and NIH 3T3 cells

Real time circadian reporter assays were performed as described previously (Ukai-Tadenuma et al., 2011) with following modifications. For the assay with *Cry1*^{-/-}:*Cry2*^{-/-} MEF, the cells in 35-mm dish were transfected with 4 µg of pGL3-P(*Per2*)-dLuc reporter plasmid and 0.03 µg of pMU2-P(*Cry1*)-FLAG-I/RRE-*Cry1* expression vector. For the AID-tagged CRY1 rescue assay, the plasmid mixture of 3µg pGL3-P(*Per2*)-dLuc, 0.03 µg pMU2-P(*Cry1*)-FLAG-I/RRE-*Cry1*-mAID, 1 µg pAID1.2str-P(CMV)-*OsTir1* was transfected. For the assay with NIH 3T3 cells, 0.4 µg of pGL3-P(*Per2*)-dLuc reporter plasmid, 0.4 µg of pMU2-P(*Cry1*)-FLAG-I/RRE-*Cry1* expression vector, and 1.2 µg of pMU2-MCS vector were transfected. After 72 hr, cells were stimulated by exchanging media for DMEM containing 30 µM (*Cry1*^{-/-}:*Cry2*^{-/-} MEF) or 10 µM (NIH 3T3) forskolin (nacalai tesque). In the AID-tagged CRY1 rescue assay, indicated concentration of NAA (N1641, Sigma-Aldrich) was added to the medium. Bioluminescence was then measured with photomultiplier detector systems (PMT-Tron for *Cry1*^{-/-}:*Cry2*^{-/-} MEF experiment shown in **Figure 1**; LM-2400, Hamamatsu Photonics, for the other experiments) at 30°C.

From the obtained bioluminescence time series, significance of rhythmicity, period length, detrended signal and relative amplitude were calculated as described previously (Ukai-Tadenuma et al., 2011). In this study, data resulting in the statistical significance ($p = 0$, most significant; $p = 1$, least significant) of circadian oscillation $p > 0.05$, or the data resulting in the relative amplitude below the 30% of averaged wild type's relative amplitude (i.e. cutoff = 0.18 for PMT-Tron assay, 0.20 for LM-2400 assay) was classified as "arrhythmic". Note that period length of the exceptionally-long period S243A:S261A mutant was calculated as the distance between the second to the third peak points. The peak points were defined using the wavelet method implemented in R software by wmtsa package, and the results were manually confirmed.

Prediction of kinases responsible for analyzed phosphorylation sites in CRY1

Prediction of kinases that catalyze the phosphorylation sites analyzed in our *Cry1*^{-/-}:*Cry2*^{-/-} MEF rescue assay was conducted by using GPS3.0, an updated version of GPS2.0 (Xue et al., 2008), running on local windows machine (<http://gps.biocuckoo.org/>), NetPhos 3.1 server (<http://www.cbs.dtu.dk/services/NetPhos/>) (Blom et al., 2004), KinasePhos2.0 server (<http://kinasephos2.mbc.nctu.edu.tw/>) (Wong et al., 2007), and Scansite 3 server (<http://scansite3.mit.edu/>), an updated version of Scansite 2 (Obenauer et al., 2003).

LC-MS quantification of the target CRY1 phosphorylation.

A CRY1 peptide (239-256), MNANLLASPTGLSPYLR and the peptides phosphorylated at S243, S247, T249 or S252 were synthesized with a peptide synthesizer Syro Wave (Biotage) using Fmoc solid-phase chemistry. Concentrations of the synthesized peptide were measured by an amino group determination method (Fields, 1972). In order to use the peptide as heavy-labeled internal standard in an MS analysis, the peptides were dimethyl-labeled with isotope-labeled formaldehyde (¹³CD₂O, ISOTEC) according to the previous report (Boersema et al., 2009). The heavy labeled peptide, which was solved in 2% acetonitrile and 0.1% TFA at 200 pmol/μL, was stored at -80°C.

For the expression of CRY1, 6 μg of *Cry1* vector or a mixture of 6 μg *Cry1* vector and 6 μg *CK1δ* vector was transfected by using 20 uL of X-tremeGENE HP (Roche) to the 5 x 10⁶ 293T cells on 90-mm dishes according to the manufacturer's instruction. The amount of transfected plasmid was adjusted to 18 μg with empty vector pMU2-MCS. After 24 hr, culture medium (DMEM/10% FBS) was replaced with 5 mL of culture medium supplemented with or without 100 μM SP600125. After 20 hr, medium in each dish was replaced with 5 mL of culture medium supplemented with 200 μM MG-132. After 4 hr, cells were collected using cell scraper and were washed with D-PBS(-).

The cell pellets were lysed in 1 mL of RIPA buffer (50 mM Tris-HCl pH 7.5, 0.3 M NaCl, 10% (v/v) glycerol, 0.5% (v/v) Triton X-100, 0.1% (v/v) NP-40, phosphatase inhibitor (Nacalai tesque, Japan) and protease inhibitor (Nacalai tesque, Japan)) by extensive sonication. The cell lysates were incubated by rotating for 20 min at 4°C, followed by centrifugation at 7,300 g for 15 min at 4°C. The supernatant were incubated with 0.1 mL of anti-FLAG M2 agarose beads (Sigma-Aldrich) with rotation for 1 h at 4°C. The beads collected by a gentle centrifugation (500 g for 2 min) were washed three times by rotating in 1.2 mL of wash buffer (20 mM Tris-HCl pH 7.5, 0.15 M NaCl, 0.25% (v/v) NP-40). The beads were rinsed with 50 mM NH₄HCO₃ solution and then incubated with 0.1 mL of 0.1 mg / mL 3X FLAG peptide (Sigma-Aldrich) solved in PTS buffer for 1 h at 4°C. After the gentle centrifugation, the supernatant (IP sample) was collected and stored at -80°C.

Immunoprecipitated CRY1 protein was enzymatically digested according to a phase-transfer surfactant (PTS) protocol (Masuda et al., 2008). The IP sample was reduced (10 mM TCEP at 37°C for 15 min) and alkylated (50 mM 2-iodoacetamide at 37°C for 15 min), and then it was diluted 5 fold by adding 50 mM NH₄HCO₃ solution followed by the digestion with 1 µg Lysyl Endopeptidase (LysC; Wako Pure Chemical Industries, Osaka, Japan) of which the reaction was performed in REDS (AMR Inc.) 400 W at 37°C for 20 min. The sample was further digested with 1 µg trypsin in the same manner. After the digestion, an equal volume of ethyl acetate was added to the sample, which was acidified with 0.5% TFA, and well mixed to transfer the detergents into an organic phase. After the centrifugation at 10,000 x g for 10 min at RT, an aqueous phase containing peptides was collected and dried with SpeedVac (Thermo Fisher Scientific). The dried peptides were solubilized in 100 µL of 2% acetonitrile and 0.1% TFA, and the peptide mixture was trapped on a C18 pipette tip prepared as previously reported (Rappsilber et al., 2007). The trapped peptides were subjected to dimethyl-labeling procedure with formaldehyde (CH₂O, Sigma) according to the previous report (Boersema et al., 2009). After the labeling, 150 µL of 15% acetonitrile

and 0.1% TFA was passed through the tip to remove the excess of 3X FLAG peptide and then the dimethyl-labeled peptides left on the tip were eluted by 150 μ L of 80% acetonitrile and 0.1% TFA. The eluent was mixed with heavy dimethyl-labeled peptides of the non-phosphorylated MNANSLLASPTGLSPYLR peptide (5 pmol) and the 4 phosphorylated versions (100 fmol each) as the internal standard for LC-MS analysis. A fiftieth of the mixture was subjected to LC-MS analysis. The remaining mixture was applied to Fe-IMAC (Immobilized Metal Ion Affinity Chromatography) according to a previous report (Narumi and Tomonaga, 2016) to enrich for phosphopeptides and then subjected to LC-MS analysis.

The LC-MS analyses were performed by selected reaction monitoring (SRM) with a triple quadrupole mass spectrometer (TSQ Vantage EMR mass spectrometer, Thermo Fisher Scientific) equipped with a captive spray ionization source (Michrom Bioresources) and an HPLC system containing a nano HPLC equipment (Advance UHPLC, Bruker Daltonics) and an HTC-PAL autosampler (CTC Analytics) with a trap column (0.3 x 5 mm, L-column, ODS, Chemicals Evaluation and Research Institute, Japan). An analytical sample solubilized in 5 μ L of 2% acetonitrile and 0.1% TFA was loaded to the LC-MS system to be separated by a gradient using mobile phases A (0.5% acetic acid) and B (0.5% acetic acid and 80% acetonitrile) at a flow rate 300 nL/min (5% to 31% B in 3 min, 31% to 35% B in 42 min, 35% to 95% B for 1 min, 95% B for 2 min, 95% to 5% B in 1 min and 5% B for 11 min) with a home-made capillary column (length of 200 mm and inner diameter of 100 μ m) packed with 2 μ m C18 resin (L-column2, Chemicals Evaluation and Research Institute, Japan) and then the eluted peptides were electrosprayed (1.6 kV) and introduced into the MS equipment (positive mode, scan width of 0.002 m/z, Q1 and Q3 resolutions of 0.7 FWHM, a cycle time of 1 sec, a gas pressure of 1.8 mTorr). SRM transitions to monitor the target peptides are shown in a **Table S5**. From the obtained raw data, SRM chromatograms for target peptides were extracted using Qual Browser of Xcaliber 2.2 (Thermo Fisher Scientific) to obtain peak areas corresponding to target peptides. The amounts of the target

peptides in a sample were determined by dividing the peak areas of the peptides derived from CRY1 by that of the corresponding internal standards.

Culture of ESCs

A conventional on-feeder culture of ESCs are as described previously (Abe et al., 2011; Kiyonari et al., 2010). The *Cry1^{-/-}:Cry2^{-/-}* mouse ESCs were established from blastocyst of *Cry1^{-/-}:Cry2^{-/-}* mouse (van der Horst et al., 1999) in 3i medium culture condition as described previously (Kiyonari et al., 2010), and their ES mouse production ability were qualified by injection into 8-cell-stage ICR embryos to select clones for further analysis. Optimized feeder-free culture condition is as below; before beginning cultivation, surface of BD PURECoat™ amine dishes were exposed to medium which contain LIF plus 6-bromoindirubin-30-oxime (BIO) (Sato et al., 2009) for more than 5 hr at 37°C with 5% CO₂. ESCs were cultured in 3i medium (Clontech Laboratories, Inc. A Takara Bio Company) on the BIO/amine-coated dish without feeder cells at 37°C with 5% CO₂.

Generation of targeted ESCs

For the conventional targeting method, the targeting vector was purified and introduced into the *Cry1^{-/-}:Cry2^{-/-}* mouse ESCs as described previously (Abe et al., 2011; Kiyonari et al., 2010; Susaki et al., 2014). For the TALEN-mediated targeting, C-terminal-truncated (+63) TALENs (Miller et al., 2011) that bind to target sequence (5'-*CTGCAACTCCAGTCTTTCTAGAAGATGGGCGGGAGTCTTCTGGGCAGGCTTA*-3', TALEN binding sequences are indicated with italics) at the ROSA26 locus were designed using TALE-NT (Doyle et al., 2012). The *Cry1^{-/-}:Cry2^{-/-}* mouse ESCs (4×10⁵ cells) were co-transfected with 0.9 μg of circular targeting vectors and 1.2 μg each of TALEN-L and TALEN-R expression vector using Xfect Transfection Reagent (Clontech Laboratories, Inc. A Takara Bio Company).

The homologously recombined, puro-resistant ESC clones were isolated for further culture and expansion. For the first screening, an aliquot of the cells was lysed and successful homologous recombination was detected by PCR of the 3' homology arm region with a pair of primers of #1 to #4 in **Figure 3C**. After expansion and stock, the ESC genome was collected and used for further confirmation of genome integrity in the targeted region. For this purpose, genomic PCR was performed by using a series of primers annealing outside the homologous recombination arms and within the inserted cassettes (**Figure 3C**). Successful targeting in the single allele was confirmed by the detection of all PCR bands from WT 5' (primers #5, 6, 9), 3' (primers #2 and #7), targeted 5' (primers #1, 5, 8, 9) and 3' homology arm regions. Primer sequences used for these screenings were summarized in **Table S6**.

The copy number of the inserted cassette was confirmed with a quantitative PCR assay using the extracted ESC genome and primers annealing to the coding sequences of the puro-resistance gene (forward primer: 5' - CTCGACATCGGCAAGGTGTG-3' , reverse primer: 5'-GGCCTTCCATCTGTTGCTGC-3') , normalized to the amount of TATA-box binding protein gene amplification (forward primer: 5'- CCCCCTCTGCACTGAAATCA-3', reverse primer: 5'-GTAGCAGCACAGAGCAAGCAA-3') using the SYBR Premix Ex Taq GC (Takara #RR071A) and the ABI PRISM 7900 (Applied Biosystems) or LightCycler 480 II (Roche) (Susaki et al., 2014). The Puro value normalized by Tbp value should be one if the single copy of inserted cassette was harbored in the genome. Note that the PuroR cassette flanked by FRT (**Figure 3C**) was not removed in this study. The selected ESC clones were injected into 8-cell-stage ICR embryos to generate ES mice (Kiyonari et al., 2010).

Estimation of host-cell contamination and chimerism of ES mouse

For the initial estimation of ES mouse production ability of the *Cry1^{-/-}:Cry2^{-/-}* ESCs,

semi-quantitative genomic PCR was performed (**Figure 3B**). The brain was dissected from sacrificed animals, frozen on a dry ice, and the hypothalamic region including the SCN was collected by cutting the frozen brain. The collected brain region was homogenized and lysed in 600 μ l of lysis buffer with Proteinase K (100 mM of NaCl, 50 mM of Tris-HCl (pH 8.0), 10 mM of EDTA, 1% of SDS, 0.6~0.7 mg/mL of Proteinase K) at 55°C for 1-2 hr, and the genomic DNA was purified and collected by phenol-chloroform purification (treated with RNase in the procedure) followed by ethanol precipitation. To detect contaminated wild-type cells in *Cry1*^{-/-}:*Cry2*^{-/-} ES mice, PCR for *Cry2* locus genotyping (wild-type allele-specific forward primer: 5'-TACCTGCGCTTTGGATGCCTCTCC-3', *Cry2*^{-/-} allele-specific forward primer: 5'-TCCCACTTTGTGTTCTAAGTACTGTGGT-3', common reverse primer: 5'-AAACCACCCATCTCTGGCTTCTCT-3') were performed in a highly sensitive condition with 200 ng of the total genomic DNA and 0.7 U of KOD-FX Neo (TOYOBO). The expected band sizes were 210 bp for wild type amplicon and 310 bp for mutant amplicon, respectively. Template genome for standard were prepared by mixing genome of wild type ICR mouse, a strain for host embryos, and a *Cry1*^{-/-}:*Cry2*^{-/-} mouse genome, purified as above, in the indicated ratios (**Figure 3A**). In this condition, the detection limit of wild-type cell contamination was estimated as ~0.001%. Coat color was used for brief estimation of the chimerism in the following ES mouse production.

Measurement of locomotor activity

For monitoring locomotor activity, C57BL/6 wild-type mice (9 weeks old), *Cry1*^{-/-}:*Cry2*^{-/-} mice (12 weeks old) (van der Horst et al., 1999), ES mice (7-10 weeks old), F1 animals of WT rescue (AS) (10 weeks old) were housed in a light-dark controlling rack (Nippon Medical & Chemical instruments Co., LTD., Japan) combined with an infrared monitoring system (NS-AS01, Neuroscience inc.) (Minami et al., 2009). They were entrained to a light-12 h: dark-12 h cycle for at least two weeks and then the locomotor activity was collected in the light-dark condition for 1-2 weeks and then in the dark-

dark condition for another 2-4 weeks.

Double-plot visualization of the collected data and calculation of chi-square (Refinetti et al., 2007; Sokolove and Bushell, 1978) were performed with ClockLab software (ActiMetrics) or our own scripts implemented in Mathematica 10 software (Wolfram Research). For calculation of chi-square, the first two weeks in the dark-dark condition was used expect for the S404D mutant (**Figure 5E**).

All experimental procedures and housing conditions were approved by the Institutional Animal Care and Use Committee of RIKEN Kobe Branch, and all of the animals were cared for and treated humanely in accordance with the institutional guidelines for experiments using animals. All mouse strains were maintained by crossing onto a C57BL/6 background.

Co-immunoprecipitation and quantification of CRY1-PER2 complex

At 24 hr before transfection, 293T cells were plated at 1×10^5 cells per 35-mm dishes. A mixture of 1 μ g of pMU2-*Cry1* (wild type or mutant series shown in **Figure 5F**) and 1 μ g of pcDNA3-*Myc-Per2* was then transfected to the 293T cells. After 48 hr, cells were collected by scraping in D-PBS(-). The cell pellet was lysed in M-PER solution (Thermo Fisher Scientific) followed by extensive sonication. The lysate was mixed with 20 μ L of anti-FLAG M2 agarose beads (Sigma-Aldrich) by rotating for 1 hr at 4°C. The beads were rinsed with 1 mL M-PER and mixed with 100 μ L of PTS buffer. The immuno-precipitants including beads were enzymatically digested as written in above section "Identification of phosphorylation sites in CRY1". The dried peptides were solubilized in 200 μ L of 2% acetonitrile and 0.1% TFA. 100 μ L of peptide mixture was taken from each wild-type/mutant CRY1 condition and mixed ("mixture" sample). The remaining 100 μ L of peptide mixture for each wild-type/mutant CRY1 condition was called "individual" sample. The peptide samples were trapped on a C18 pipette tip prepared as previously reported (Rappsilber et al., 2007), followed by dimethyl-

labeling according to the previous report (Boersema et al., 2009). Formaldehyde (CH₂O, Sigma) was used to label the mixture sample ("light-label"), and isotope-labeled formaldehyde (¹³CD₂O, ISOTECH) was used to label the individual samples ("heavy-label"). The dimethyl-labeled peptides on the tip were eluted by 80% acetonitrile and 0.1% TFA. Then, equal amount of eluted solution of light-labeled mixture sample was added to each heavy-labeled individual sample (wild-type or mutant CRY1 series). Thus, the relative amount of immuno-precipitants in the individual samples can be compared to each other by using the equally-added light-labeled samples as a standard.

The samples were analyzed by data-dependent MS/MS with a Q-FT mass spectrometer (Q-Exactive mass spectrometer, Thermo Fisher Scientific) equipped with an HPLC system containing a nano HPLC equipment (Advance UHPLC, Bruker Daltonics) and an HTC-PAL autosampler (CTC Analytics) with a trap column (0.3 x 5 mm, L-column, ODS, Chemicals Evaluation and Research Institute, Japan). An analytical sample solubilized in 20 µL of 2% acetonitrile and 0.1% TFA was loaded to the LC-MS system to be separated by a gradient using mobile phases A (0.5% acetic acid) and B (0.5% acetic acid and 80% acetonitrile) at a flow rate 300 nL/min (4% to 36% B in 55 min, 36% to 95% B in 1 min, 95% B for 5 min, 95% to 4% B in 1 min and 5% B for 8 min) with a home-made capillary column (length of 200 mm and inner diameter of 100 µm) packed with 2 µm C18 resin (L-column2, Chemicals Evaluation and Research Institute, Japan) and then the eluted peptides were electrosprayed (1.8-2.3 kV) and introduced into the MS equipment (positive ion mode, data-dependent MS/MS). The obtained raw data was subjected to database search with SequestHT algorithm running on Proteome Discoverer (Thermo Fisher Scientific).

The area of precursor ions corresponding to the following four peptides derived from CRY1 were then manually quantified by chromatogram generated with Xcalibur 2.2 software (Thermo Fisher Scientific): IATEAGVEVIVR (z = 2), YIYDPWNAPEGIQk (z = 2), AWWANFERPR (z = 2), and KLATEAGVEVIVR (z = 2).

For each peptide, the area of heavy-labeled peptide (H) and light-labeled peptide (L) were quantified, and the averaged H/L ratio is used as the “relative amount of CRY1” involved in each “individual” sample. Similarly, the area of precursor ions corresponding to following three peptides derived from PER2 were also manually quantified: DLQAVLK ($z = 2$), FVEFLAPHDVSVFHHSYTPYK ($z = 3$), and ILQAGGQPFDYSPYR ($z = 2$). The H/L ratio of each PER2-derived peptide was calculated and then divided by the relative amount of CRY1. Thus, the relative value of (co-immunoprecipitated PER2-derived peptide) / (immunoprecipitated CRY1) could be obtained for each PER2 derived peptide and plotted in **Figure 5F**.

CRY1 half-life assay

Cry1^{-/-}:Cry2^{-/-} MEF were plated at 4×10^5 cells per 35-mm dish. After 24 hr, 1 μg of pMU2-*Cry1::luciferase* and 1 μg of pMU2-MCS were transfected with FuGene6 (Promega) according to the manufacture’s instruction. After 72 hr, the medium was replaced with DMEM (21063-029, Life technologies) supplemented with 0.1 mM luciferin (Promega). Bioluminescence was measured in LM-2400 (Hamamatsu Photonics) at 30°C. After 96 hr, 400 $\mu\text{g}/\text{mL}$ cycloheximide (Sigma-Aldrich) was added. Half-life of luciferase signal was calculated by fitting the time series of 0 – 300 min after the cycloheximide addition to the equation,

$$X(t) = a \cdot e^{-k \cdot t} + (1 - a)$$

, where $X(t)$ is the time series of luciferase signal, and a and k are the fitting parameters.

The half-life time is given as

$$t_{half-time} = \frac{\ln\left(1 - \frac{0.5}{a}\right)}{k}$$

E-box repression assay

Transcription repression assay was performed as described previously (Khan et al., 2012) except for that 1×10^5 *Cry1*^{-/-}:*Cry2*^{-/-} MEFs were plated onto one well of a 24-well plate, and total plasmid amount was adjusted to 810 ng per well (a mixture of 400 ng pMU2-P(*Cry1*)-FLAG-I/RRE-*Cry1* vector, 400 ng pGL3-P(*Per2*)-d*Luc*, and 10 ng phRL-SV40 plasmid). In the assay shown in **Figure S4D** (+TIR condition), a mixture of 200 ng pMU2-P(*Cry1*)-FLAG-I/RRE-*Cry1*(-mAID) vector, 200ng of pAID1.2str-P(CMV)-*OsTir1*, 400 ng pGL3-P(*Per2*)-d*Luc*, and 10 ng phRL-SV40 plasmid was transfected.

Sequence alignment and molecular phylogenetic analysis

The amino acid sequences for cryptochrome superfamily were collected from Swiss-Prot database with search keywords “cryptochrome”, “6 4 photolyase”, or “CPD photolyase”. Proteins that are not involved in the cryptochrome superfamily were manually excluded. The sequence dataset was aligned by MUSCLE algorithm (Edgar, 2004) running on MEGA7 software (Kumar et al., 2016). A phylogenetic tree for cryptochrome superfamily proteins were calculated by the MEGA7 using Maximum Likelihood method based on the JTT matrix-based model (Jones et al., 1992). A sequence logo is generated through WebLogo 3.5.0 website (Crooks et al., 2004).

Protein structural analyses

All images for protein structures were built by using PyMOL software (Schrodinger, LLC). For the calculation of electrostatic potential, PDB file was converted to PQR file by the PDB2PQR web service with PARSE forcefiled (Dolinsky et al., 2007; Dolinsky et al., 2004). pH 7 was chosen for pKa calculation. The PQR file was then used for the generation of electrostatic potential map by using APBS software (Baker et al., 2001) running on PyMOL software.

Statistical analysis and data processing

All statistical analysis and data processing were done in R 3.2.0, Mathematica 10 (Wolfram Research), or Excel 2013 (Microsoft).

SUPPLEMENTAL REFERENCES

- Abe, T., Kiyonari, H., Shioi, G., Inoue, K., Nakao, K., Aizawa, S., and Fujimori, T. (2011). Establishment of conditional reporter mouse lines at ROSA26 locus for live cell imaging. *Genesis* 49, 579-590.
- Aubert, C., Vos, M.H., Mathis, P., Eker, A.P., and Brettel, K. (2000). Intraprotein radical transfer during photoactivation of DNA photolyase. *Nature* 405, 586-590.
- Baker, N.A., Sept, D., Joseph, S., Holst, M.J., and McCammon, J.A. (2001). Electrostatics of nanosystems: application to microtubules and the ribosome. *Proc Natl Acad Sci U S A* 98, 10037-10041.
- Blom, N., Sicheritz-Ponten, T., Gupta, R., Gammeltoft, S., and Brunak, S. (2004). Prediction of post-translational glycosylation and phosphorylation of proteins from the amino acid sequence. *Proteomics* 4, 1633-1649.
- Boersema, P.J., Raijmakers, R., Lemeer, S., Mohammed, S., and Heck, A.J. (2009). Multiplex peptide stable isotope dimethyl labeling for quantitative proteomics. *Nat Protoc* 4, 484-494.
- Bothwell, A.L., Paskind, M., Reth, M., Imanishi-Kari, T., Rajewsky, K., and Baltimore, D. (1981). Heavy chain variable region contribution to the NPb family of antibodies: somatic mutation evident in a gamma 2a variable region. *Cell* 24, 625-637.
- Crooks, G.E., Hon, G., Chandonia, J.M., and Brenner, S.E. (2004). WebLogo: a sequence logo generator. *Genome Res* 14, 1188-1190.
- Czarna, A., Berndt, A., Singh, H.R., Grudziecki, A., Ladurner, A.G., Timinszky, G., Kramer, A., and Wolf, E. (2013). Structures of *Drosophila* cryptochrome and mouse cryptochrome1 provide insight into circadian function. *Cell* 153, 1394-1405.
- Dolinsky, T.J., Czodrowski, P., Li, H., Nielsen, J.E., Jensen, J.H., Klebe, G., and Baker, N.A. (2007). PDB2PQR: expanding and upgrading automated preparation of biomolecular structures for molecular simulations. *Nucleic Acids Res* 35, W522-525.
- Dolinsky, T.J., Nielsen, J.E., McCammon, J.A., and Baker, N.A. (2004). PDB2PQR: an automated pipeline for the setup of Poisson-Boltzmann electrostatics calculations. *Nucleic Acids Res* 32, W665-667.
- Doyle, E.L., Booher, N.J., Standage, D.S., Voytas, D.F., Brendel, V.P., Vandyk, J.K., and Bogdanove, A.J. (2012). TAL Effector-Nucleotide Targeter (TALE-NT) 2.0: tools for TAL effector design and target prediction. *Nucleic Acids Res* 40, W117-122.
- Edgar, R.C. (2004). MUSCLE: multiple sequence alignment with high accuracy and high throughput. *Nucleic Acids Res* 32, 1792-1797.
- Fields, R. (1972). [38] The rapid determination of amino groups with TNBS. *Methods Enzymol* 25, 464-468.
- Hitomi, K., DiTacchio, L., Arvai, A.S., Yamamoto, J., Kim, S.T., Todo, T., Tainer,

J.A., Iwai, S., Panda, S., and Getzoff, E.D. (2009). Functional motifs in the (6-4) photolyase crystal structure make a comparative framework for DNA repair photolyases and clock cryptochromes. *Proc Natl Acad Sci U S A* 106, 6962-6967.

Hitomi, K., Nakamura, H., Kim, S.T., Mizukoshi, T., Ishikawa, T., Iwai, S., and Todo, T. (2001). Role of two histidines in the (6-4) photolyase reaction. *J Biol Chem* 276, 10103-10109.

Isojima, Y., Nakajima, M., Ukai, H., Fujishima, H., Yamada, R.G., Masumoto, K.H., Kiuchi, R., Ishida, M., Ukai-Tadenuma, M., Minami, Y., *et al.* (2009). CKIepsilon/delta-dependent phosphorylation is a temperature-insensitive, period-determining process in the mammalian circadian clock. *Proc Natl Acad Sci U S A* 106, 15744-15749.

Jones, D.T., Taylor, W.R., and Thornton, J.M. (1992). The Rapid Generation of Mutation Data Matrices from Protein Sequences. *Computer Applications in the Biosciences* 8, 275-282.

Khan, S.K., Xu, H., Ukai-Tadenuma, M., Burton, B., Wang, Y., Ueda, H.R., and Liu, A.C. (2012). Identification of a novel cryptochrome differentiating domain required for feedback repression in circadian clock function. *J Biol Chem* 287, 25917-25926.

Kiyonari, H., Kaneko, M., Abe, S., and Aizawa, S. (2010). Three inhibitors of FGF receptor, ERK, and GSK3 establishes germline-competent embryonic stem cells of C57BL/6N mouse strain with high efficiency and stability. *Genesis* 48, 317-327.

Kubota, T., Nishimura, K., Kanemaki, M.T., and Donaldson, A.D. (2013). The Elg1 replication factor C-like complex functions in PCNA unloading during DNA replication. *Mol Cell* 50, 273-280.

Kumar, S., Stecher, G., and Tamura, K. (2016). MEGA7: Molecular Evolutionary Genetics Analysis Version 7.0 for Bigger Datasets. *Mol Biol Evol* 33, 1870-1874.

Li, J., Liu, Z., Tan, C., Guo, X., Wang, L., Sancar, A., and Zhong, D. (2010). Dynamics and mechanism of repair of ultraviolet-induced (6-4) photoproduct by photolyase. *Nature* 466, 887-890.

Liu, Z., Tan, C., Guo, X., Kao, Y.T., Li, J., Wang, L., Sancar, A., and Zhong, D. (2011). Dynamics and mechanism of cyclobutane pyrimidine dimer repair by DNA photolyase. *Proc Natl Acad Sci U S A* 108, 14831-14836.

Masuda, T., Tomita, M., and Ishihama, Y. (2008). Phase transfer surfactant-aided trypsin digestion for membrane proteome analysis. *J Proteome Res* 7, 731-740.

Maul, M.J., Barends, T.R., Glas, A.F., Cryle, M.J., Domratcheva, T., Schneider, S., Schlichting, I., and Carell, T. (2008). Crystal structure and mechanism of a DNA (6-4) photolyase. *Angew Chem Int Ed Engl* 47, 10076-10080.

Miller, J.C., Tan, S., Qiao, G., Barlow, K.A., Wang, J., Xia, D.F., Meng, X., Paschon, D.E., Leung, E., Hinkley, S.J., *et al.* (2011). A TALE nuclease architecture for

efficient genome editing. *Nat Biotechnol* 29, 143-148.

Minami, Y., Kasukawa, T., Kakazu, Y., Iigo, M., Sugimoto, M., Ikeda, S., Yasui, A., van der Horst, G.T., Soga, T., and Ueda, H.R. (2009). Measurement of internal body time by blood metabolomics. *Proc Natl Acad Sci U S A* 106, 9890-9895.

Nangle, S., Xing, W., and Zheng, N. (2013). Crystal structure of mammalian cryptochrome in complex with a small molecule competitor of its ubiquitin ligase. *Cell Res* 23, 1417-1419.

Nangle, S.N., Rosensweig, C., Koike, N., Tei, H., Takahashi, J.S., Green, C.B., and Zheng, N. (2014). Molecular assembly of the period-cryptochrome circadian transcriptional repressor complex. *Elife* 3, e03674.

Narumi, R., Shimizu, Y., Ukai-Tadenuma, M., Ode, K.L., Kanda, G.N., Shinohara, Y., Sato, A., Matsumoto, K., and Ueda, H.R. (2016). Mass spectrometry-based absolute quantification reveals rhythmic variation of mouse circadian clock proteins. *Proc Natl Acad Sci U S A* 113, E3461-3467.

Narumi, R., and Tomonaga, T. (2016). Quantitative Analysis of Tissue Samples by Combining iTRAQ Isobaric Labeling with Selected/Multiple Reaction Monitoring (SRM/MRM). *Methods Mol Biol* 1355, 85-101.

Nash, P., Tang, X., Orlicky, S., Chen, Q., Gertler, F.B., Mendenhall, M.D., Sicheri, F., Pawson, T., and Tyers, M. (2001). Multisite phosphorylation of a CDK inhibitor sets a threshold for the onset of DNA replication. *Nature* 414, 514-521.

Obenauer, J.C., Cantley, L.C., and Yaffe, M.B. (2003). Scansite 2.0: Proteome-wide prediction of cell signaling interactions using short sequence motifs. *Nucleic Acids Res* 31, 3635-3641.

Orlando, S.J., Santiago, Y., DeKolver, R.C., Freyvert, Y., Boydston, E.A., Moehle, E.A., Choi, V.M., Gopalan, S.M., Lou, J.F., Li, J., *et al.* (2010). Zinc-finger nuclease-driven targeted integration into mammalian genomes using donors with limited chromosomal homology. *Nucleic Acids Res* 38, e152.

Orlicky, S., Tang, X., Willems, A., Tyers, M., and Sicheri, F. (2003). Structural basis for phosphodependent substrate selection and orientation by the SCFCdc4 ubiquitin ligase. *Cell* 112, 243-256.

Rappsilber, J., Mann, M., and Ishihama, Y. (2007). Protocol for micro-purification, enrichment, pre-fractionation and storage of peptides for proteomics using StageTips. *Nat Protoc* 2, 1896-1906.

Refinetti, R., Lissen, G.C., and Halberg, F. (2007). Procedures for numerical analysis of circadian rhythms. *Biol Rhythm Res* 38, 275-325.

Sadeghian, K., Bocola, M., Merz, T., and Schutz, M. (2010). Theoretical study on the repair mechanism of the (6-4) photolesion by the (6-4) photolyase. *J Am Chem Soc* 132, 16285-16295.

Sato, H., Amagai, K., Shimizukawa, R., and Tamai, Y. (2009). Stable generation of serum- and feeder-free embryonic stem cell-derived mice with full germline-competency by using a GSK3 specific inhibitor. *Genesis* 47, 414-422.

Sato, T.K., Yamada, R.G., Ukai, H., Baggs, J.E., Miraglia, L.J., Kobayashi, T.J., Welsh, D.K., Kay, S.A., Ueda, H.R., and Hogenesch, J.B. (2006). Feedback repression is required for mammalian circadian clock function. *Nat Genet* 38, 312-319.

Schmalen, I., Reischl, S., Wallach, T., Klemz, R., Grudziecki, A., Prabu, J.R., Benda, C., Kramer, A., and Wolf, E. (2014). Interaction of Circadian Clock Proteins CRY1 and PER2 Is Modulated by Zinc Binding and Disulfide Bond Formation. *Cell* 157, 1203-1215.

Sokolove, P.G., and Bushell, W.N. (1978). The chi square periodogram: its utility for analysis of circadian rhythms. *J Theor Biol* 72, 131-160.

Stanewsky, R., Kaneko, M., Emery, P., Beretta, B., Wager-Smith, K., Kay, S.A., Rosbash, M., and Hall, J.C. (1998). The cryb mutation identifies cryptochrome as a circadian photoreceptor in *Drosophila*. *Cell* 95, 681-692.

Susaki, E.A., Tainaka, K., Perrin, D., Kishino, F., Tawara, T., Watanabe, T.M., Yokoyama, C., Onoe, H., Eguchi, M., Yamaguchi, S., *et al.* (2014). Whole-brain imaging with single-cell resolution using chemical cocktails and computational analysis. *Cell* 157, 726-739.

Tainaka, K., Kubota, S.I., Suyama, T.Q., Susaki, E.A., Perrin, D., Ukai-Tadenuma, M., Ukai, H., and Ueda, H.R. (2014). Whole-body imaging with single-cell resolution by tissue decolorization. *Cell* 159, 911-924.

Ukai-Tadenuma, M., Yamada, R.G., Xu, H., Ripperger, J.A., Liu, A.C., and Ueda, H.R. (2011). Delay in feedback repression by cryptochrome 1 is required for circadian clock function. *Cell* 144, 268-281.

Ukai, H., Kobayashi, T.J., Nagano, M., Masumoto, K.H., Sujino, M., Kondo, T., Yagita, K., Shigeyoshi, Y., and Ueda, H.R. (2007). Melanopsin-dependent photoperurbation reveals desynchronization underlying the singularity of mammalian circadian clocks. *Nat Cell Biol* 9, 1327-1334.

van der Horst, G.T., Muijtjens, M., Kobayashi, K., Takano, R., Kanno, S., Takao, M., de Wit, J., Verkerk, A., Eker, A.P., van Leenen, D., *et al.* (1999). Mammalian Cry1 and Cry2 are essential for maintenance of circadian rhythms. *Nature* 398, 627-630.

Wong, Y.H., Lee, T.Y., Liang, H.K., Huang, C.M., Wang, T.Y., Yang, Y.H., Chu, C.H., Huang, H.D., Ko, M.T., and Hwang, J.K. (2007). KinasePhos 2.0: a web server for identifying protein kinase-specific phosphorylation sites based on sequences and coupling patterns. *Nucleic Acids Res* 35, W588-594.

Xing, W., Busino, L., Hinds, T.R., Marionni, S.T., Saifee, N.H., Bush, M.F., Pagano,

M., and Zheng, N. (2013). SCF(FBXL3) ubiquitin ligase targets cryptochromes at their cofactor pocket. *Nature* 496, 64-68.

Xue, Y., Ren, J., Gao, X., Jin, C., Wen, L., and Yao, X. (2008). GPS 2.0, a tool to predict kinase-specific phosphorylation sites in hierarchy. *Mol Cell Proteomics* 7, 1598-1608.